

8-Substituted Pyrido[3,4-*d*]pyrimidin-4(3*H*)-one Derivatives As Potent, Cell Permeable, KDM4 (JMJD2) and KDM5 (JARID1) Histone Lysine Demethylase Inhibitors

Vassilios Bavetsias,^{*,†} Rachel M. Lanigan,[†] Gian Filippo Ruda,^{‡,§} Butrus Atrash,[†] Mark G. McLaughlin,[†] Anthony Tumber,^{‡,§} N. Yi Mok,[†] Yann-Vaï Le Bihan,[†] Sally Dempster,[†] Katherine J. Boxall,[†] Fiona Jeganathan,[†] Stephanie B. Hatch,^{‡,§} Pavel Savitsky,[‡] Srikannathasan Velupillai,[‡] Tobias Krojer,[‡] Katherine S. England,^{‡,§} Jimmy Sejberg,[†] Ching Thai,[†] Adam Donovan,[†] Akos Pal,[†] Giuseppe Scozzafava,^{‡,§} James M. Bennett,^{‡,§} Akane Kawamura,^{||} Catrine Johansson,^{‡,⊥} Aleksandra Szykowska,[‡] Carina Gileadi,[‡] Nicola A. Burgess-Brown,[‡] Frank von Delft,^{‡,#,∇} Udo Oppermann,^{‡,⊥} Zoe Walters,[○] Janet Shipley,[○] Florence I. Raynaud,[†] Susan M. Westaway,[◆] Rab K. Prinjha,[◆] Oleg Fedorov,^{‡,§} Rosemary Burke,[†] Christopher J. Schofield,^{||} Isaac M. Westwood,[†] Chas Bountra,[‡] Susanne Müller,^{‡,§} Rob L. M. van Montfort,[†] Paul E. Brennan,^{*,‡,§} and Julian Blagg^{*,†}

[†]Cancer Research UK Cancer Therapeutics Unit, The Institute of Cancer Research, 15 Cotswold Road, London SM2 5NG, U.K.

[‡]Structural Genomics Consortium (SGC), University of Oxford, ORCRB Roosevelt Drive, Oxford OX3 7DQ, U.K.

[§]Target Discovery Institute (TDI), Nuffield Department of Medicine, University of Oxford, NDMRB Roosevelt Drive, Oxford OX3 7FZ, U.K.

^{||}Chemistry Research Laboratory, University of Oxford, Mansfield Road, Oxford OX1 3TA, U.K.

[⊥]Botnar Research Centre, NIHR Oxford Biomedical Research Unit, Oxford OX3 7LD, U.K.

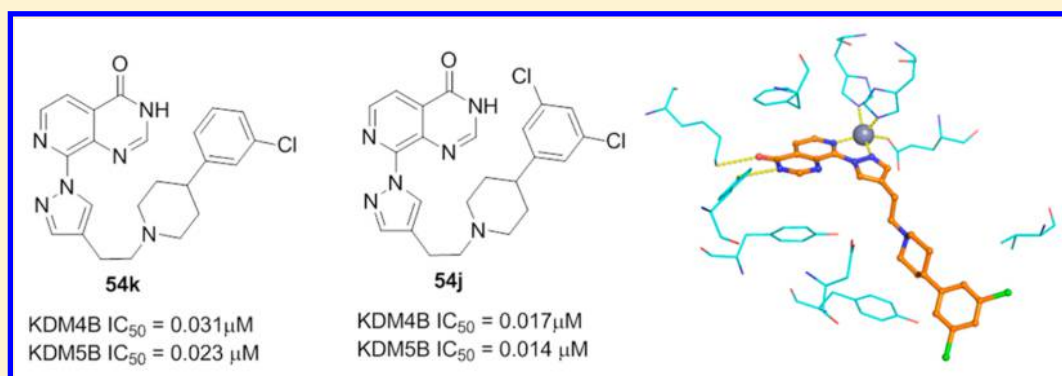
[#]Diamond Light Source (DLS), Harwell Science and Innovation Campus, Didcot OX11 0DE, U.K.

[∇]Department of Biochemistry, University of Johannesburg, Auckland Park 2006, South Africa

[○]Divisions of Molecular Pathology and Cancer Therapeutics, The Institute of Cancer Research, London SM2 5NG, U.K.

[◆]Epinova Discovery Performance Unit, Medicines Research Centre, GlaxoSmithKline R&D, Stevenage SG1 2NY, U.K.

S Supporting Information



ABSTRACT: We report the discovery of *N*-substituted 4-(pyridin-2-yl)thiazole-2-amine derivatives and their subsequent optimization, guided by structure-based design, to give 8-(1*H*-pyrazol-3-yl)pyrido[3,4-*d*]pyrimidin-4(3*H*)-ones, a series of potent JmjC histone *N*-methyl lysine demethylase (KDM) inhibitors which bind to Fe(II) in the active site. Substitution from C4 of the pyrazole moiety allows access to the histone peptide substrate binding site; incorporation of a conformationally constrained 4-phenylpiperidine linker gives derivatives such as **54j** and **54k** which demonstrate equipotent activity versus the KDM4 (JMJD2) and KDM5 (JARID1) subfamily demethylases, selectivity over representative exemplars of the KDM2, KDM3, and KDM6 subfamilies, cellular permeability in the Caco-2 assay, and, for **54k**, inhibition of H3K9Me₃ and H3K4Me₃ demethylation in a cell-based assay.

Special Issue: Epigenetics

Received: October 18, 2015

Published: January 7, 2016

INTRODUCTION

Post-translational histone modifications, which include lysine or arginine methylation, play a pivotal role in maintaining chromatin architecture and regulating transcription.¹ Histone lysine methylation is a reversible process; the removal of methyl groups is catalyzed by two classes of histone lysine demethylases (KDMs): the flavin-dependent lysine specific demethylase (LSD/KDM1) family that demethylate mono- and dimethyl lysine substrates, and the larger class of Fe(II) and 2-oxoglutarate (2OG)-dependent enzymes which can additionally convert trimethyl lysine substrates to their dimethyl forms.^{2–4} The 2OG-dependent KDMs belong to the Jumoni C (JmjC) domain containing subfamily of such enzymes and have a catalytic site wherein methylated lysine substrates can be oxidized to hemiaminal intermediates, which subsequently decompose to the corresponding demethylated lysine and formaldehyde.^{2,4}

Human JmjC histone demethylases comprise five subfamilies. The KDM4 (JMJD2) subfamily consists of six members KDM4A–F; KDM4E and KDM4F are believed to be pseudogenes although demethylase activity has been demonstrated when KDM4E is ectopically expressed.^{5,6} KDM4A–C contain PHD and Tudor domains as well as a single JmjC domain that catalyzes demethylation of histone substrates H3K9Me₃/Me₂, H3K36Me₃/Me₂, and H1.4K26Me₃.^{1,5,7,8} KDM4D is distinguished from KDM4A–C in terms of its domains (it lacks both the PHD and Tudor domains), its selectivity for demethylation of H3K9Me₃/Me₂ over H3K36Me₃/Me₂,^{5,7} and also its ability to demethylate both the dimethylated and trimethylated forms of H1.4K26.^{7,9}

Emerging evidence suggests that KDM4 subfamily members play an important role in cancer initiation and progression; various studies have shown overexpression of KDM4A–C in a range of human malignancies.^{5,7,10–12} For example, KDM4B and KDM4C are reported to be overexpressed in breast cancer;^{10,11} KDM4B knockdown in ER-positive ZR-75-1 breast cancer cells impaired growth in a human tumor xenograft model,¹¹ and KDM4B knockdown in human gastric cancer cells also suppressed growth in a human tumor xenograft model.¹² KDM4B gene expression is high in rhabdomyosarcomas and has been associated with poor prognosis in neuroblastoma.^{13,14} A recent report demonstrates a role for KDM4A in site-specific copy gain of chromosomal domains (e.g., 1q12) and rereplication of regions amplified in tumors;¹⁵ furthermore, a coding single-nucleotide polymorphism (SNP) in KDM4A was shown to associate with worse outcome in non-small cell lung cancer patients and with increased sensitivity to mTOR inhibitors.^{16,17}

The KDM5 subfamily are histone H3 lysine 4 (H3K4) demethylases and have been implicated in cancer progression in several tumor types.^{18,19} Along with members of the KDM4 family, KDM5B and KDM5C have been shown to play a

role in breast and prostate cancer, respectively. KDM5B has been implicated in several subtypes of breast cancer,^{20,21} while KDM5C has been shown to be an independent prognostic factor in prostate cancer.²² JmjC KDM activity is also associated with diseases other than cancer;²³ for example, KDM6B/A (JMJD3/UTX)-mediated demethylation of H3K27 has been reported as a critical determinant of pro-inflammatory gene activation in human primary macrophages.²⁴ Thus, JmjC KDMs have emerged as important therapeutic targets, particularly for the treatment human malignancies.^{7,23,25}

A range of small-molecule inhibitors of JmjC KDMs has been reported, the majority of which are 2OG-competitive and coordinate to Fe(II) in the catalytic site,^{26–34} for example, compounds 1–3^{32–34} (Figure 1). Many of these early histone demethylase modulators lack human 2OG oxygenase specificity³² and possess a carboxylic acid moiety which may limit cell permeability. As a result, such compounds are suboptimal chemical tools with which to better understand the biological role of specific KDM4 subfamily enzymes in disease and normal development, in particular, to study the importance of JmjC domain KDM activity within the context of full length KDM4 proteins wherein the noncatalytic domains may play a role in chromatin localization or scaffolding functions. In an attempt to overcome the poor cell permeability of inhibitors bearing a carboxylic acid, corresponding ester prodrugs have been investigated in some cases; for example, for the KDM6-selective inhibitor 4 (GSK-J1, Figure 1) where the corresponding ethyl ester prodrug found utility in a cellular context.²⁴

Extensive interest in the KDM4/5 subfamilies in the progression of human cancers, and the well-defined catalytic mechanism for JmjC KDMs, prompted us to initiate a program to identify histone KDM inhibitors, and in particular potent, cell permeable, and selective inhibitors of the KDM4 subfamily with which to further explore the potential of such compounds as anticancer agents. Herein, we report the identification of a 4-(pyridin-2-yl)thiazol-2-amine series as KDM inhibitors from a high throughput screening (HTS) campaign and their subsequent structure-based optimization into potent, cell permeable dual inhibitors of the KDM4 and KDM5 subfamilies.

CHEMISTRY

Synthesis of the HTS-derived series of *N*-(4-(pyridin-2-yl)thiazol-2-yl)benzamides 7a–d (Scheme 1A, Table 1) was achieved by EDCI/HOBT-mediated coupling of commercially available benzoic acids 6 with 4-(pyridin-2-yl)thiazol-2-amine (5). This procedure has recently been reported for the preparation of 2-aminothiazole derivatives as antimycobacterial and antiplasmodial agents.³⁵ 4-(Pyridin-3-yl)thiazole derivatives 9a,b (Scheme 1B, Table 2) were obtained from commercially

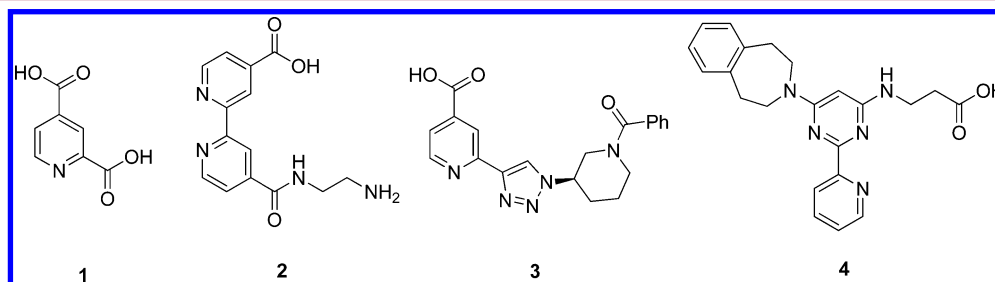
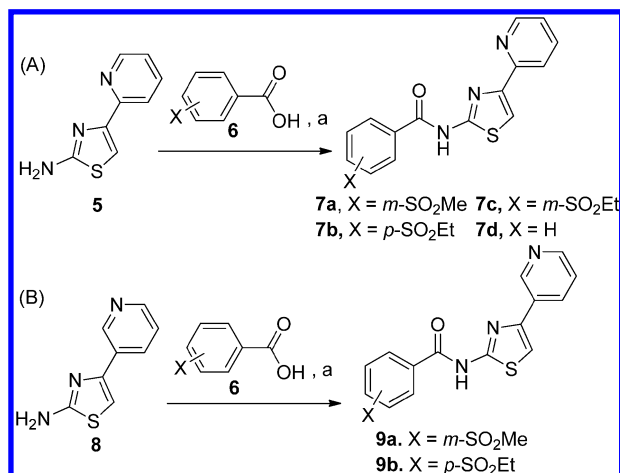


Figure 1. Pyridine-based histone demethylase inhibitors.

Scheme 1^a

^aReagents and conditions: (a) EDCl, 1-hydroxybenzotriazole, CH₂Cl₂ or CH₂Cl₂/DMF, room temp, 3.5–36 h, (7a = 33%, 7b = 25%, 7c = 40%, 7d = 50%, 9a = 28%, 9b = 16%).

available 4-(pyridin-3-yl)thiazol-2-amine (8) by a procedure analogous to that described for the synthesis of 7a–d.

Syntheses of 2-aminothiazoles 15 and 16 and 2-benzamidothiazole 19 are shown in Scheme 2. Treatment of methyl 2-bromoisonicotinate (10) with stannane 11 under Pd-catalyzed conditions gave methyl 2-(1-ethoxyvinyl)isonicotinate (12); subsequent reaction with *N*-bromosuccinimide afforded bromide 13. Thiazole ring formation to give the 2,4-disubstituted thiazole 14 was effected by reacting 13 with *N*-Boc-thiourea in the presence of trimethylamine, and subsequent removal of the protecting groups provided 2-aminothiazole derivative 15. Treatment of 2,4-disubstituted thiazole 14 with ammonia in methanol at 80 °C followed by acid-mediated removal of the

N-Boc protecting group provided the primary amide 16. Access to 2-benzamidothiazole 19 was achieved by coupling of benzoyl chloride with 2-aminothiazole 17 followed by ester hydrolysis under alkaline conditions (Scheme 2).

Preparation of 22 followed an alternative approach whereby the thiazole ring was introduced directly via a Stille cross-coupling reaction (Scheme 3). Access to 24, a key intermediate for the preparation of 25, was achieved by bromination of 23 followed by 2-methylthiazole ring formation in a manner analogous to the preparation of 14 (Scheme 3).

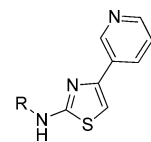
2-Benzylaminomethylpyridine (30b) and 2-furanylmethylamino derivative (30a)³⁶ were prepared from pyridine-2,4-dicarboxylate (26) in a four-step sequence (Scheme 4). Esterification of 26, followed by DIBAL-mediated selective reduction of the carboxylic acid ester in the 2-position of 27 afforded aldehyde 28. Reductive amination of aldehyde 28 with either benzylamine or 2-aminomethylfuran in the presence of sodium triacetoxyborohydride led to ester derivatives 29a,b, which were subsequently hydrolyzed to the corresponding carboxylates 30a,b with lithium hydroxide (Scheme 4).

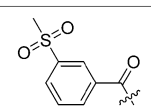
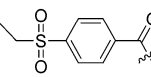
8-Chloropyrido[3,4-*d*]pyrimidin-4(3*H*)-one (34), the key intermediate for the synthesis of thiazole-C4 substituted derivative 37, 2,4-disubstituted thiazole 40 and subsequent SAR exploration (vide infra), was prepared in three steps from methyl-3-amino-2-chloroisonicotinate (31) (Scheme 5). Ester hydrolysis afforded 32 which was converted into the primary amide 33 via the corresponding acid chloride; subsequent ring formation was effected upon treatment with triethyl orthoformate (Scheme 5). A SEM-protecting group was introduced by reacting 34 with SEM-Cl in the presence of potassium carbonate to give protected pyridopyrimidinone 35. Bromide 39, a key intermediate for the preparation of 40, was obtained from 34 in a manner analogous to that described for 13 (Scheme 2). 2-Aminothiazole formation to afford 40 was achieved by reacting

Table 1. *N*-Substituted 4-(Pyridin-2-yl)thiazole-2-amine Derivatives^b

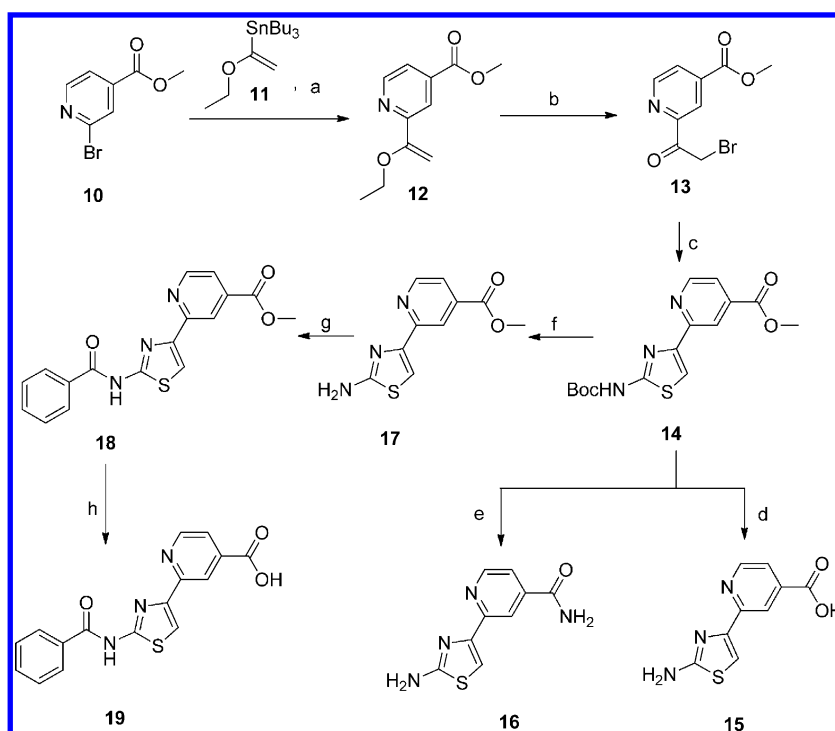
Compound	R	KDM4A IC ₅₀ (μM)	KDM4B IC ₅₀ (μM)	KDM5B IC ₅₀ (μM)	KDM5C IC ₅₀ (μM)
7a		16.7±3.9	11.3±1.4	29.7	71.9
7b		10.9±4.3	6.4±0.8	22.7	52.8
7c		13.2	10.9±0.3	52.6 ^a	65% inh at 100 μM ^a
7d		20.9	12.1	51.2 ^a	62% inh at 100 μM ^a
5	H	6% inh at 100 μM	30% inh at 100 μM	Not active at 100 μM	Not active at 100 μM

^aResults are from a single experiment. ^bResults are mean values of two independent determinations or mean (±SD) for *n* > 2 unless specified otherwise.

Table 2. *N*-Substituted 4-(Pyridin-3-yl)thiazole-2-amine Derivatives^a


Compound	R	KDM4A, inhibition at 100 μ M	KDM4B, inhibition at 100 μ M	KDM5B, inhibition at 100 μ M	KDM5C, inhibition at 100 μ M
8	H	Not active	10%	17%	8%
9a		Not active	Not active	36%	14%
9b		Not active	Not active	43%	21%

^aResults are mean values of two independent determinations unless specified otherwise.

Scheme 2^a

^aReagents and conditions: (a) Pd(PPh₃)₄, 1,4-dioxane, reflux, 18 h, 65%; (b) *N*-bromosuccinimide, 10% water in THF, room temp, 1 h, 61%; (c) *N*-Boc-thiourea, Et₃N, EtOH, reflux, 1 h, 56%; (d) (i) 4 M HCl in dioxane, room temp, 1 h, (ii) THF/H₂O, NaOH, room temp, 1 h, 55%; (e) (i) 7 M NH₃ in MeOH, 80 °C, 18 h, (ii) 4 M HCl in dioxane, room temp, 1 h, 91%; (f) 4 M HCl in dioxane, room temp, 1 h, 83%; (g) benzoyl chloride, CH₂Cl₂, Et₃N, room temp, 2 h, 35%; (h) THF/MeOH, H₂O, NaOH, room temp, 1 h, 40%.

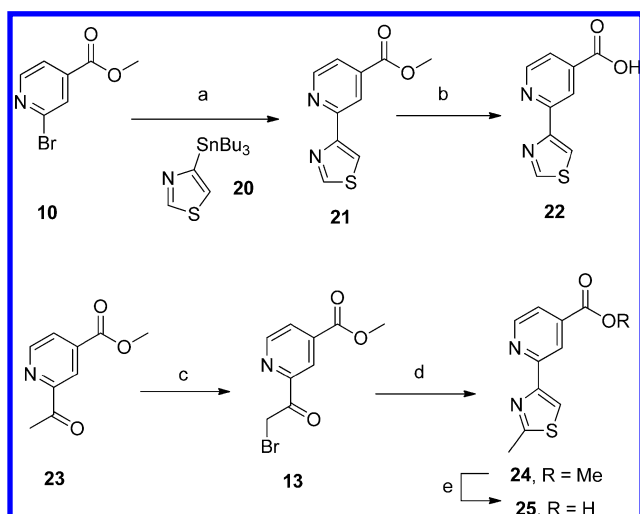
39 with thiourea in the presence of Et₃N. Compound 37 was prepared from 34 by a Stille cross-coupling reaction to introduce the thiazole ring followed by removal of the SEM protecting group under acidic conditions (Scheme 5).

8-Chloropyrido[3,4-*d*]pyrimidin-4(3*H*)-one (34) was also employed for the synthesis of pyrazolyl derivatives 41a,b by a Suzuki cross-coupling reaction with (1*H*-pyrazol-3-yl)boronic acid or ((*N*-methyl)pyrazol-3-yl)boronic acid pinacol ester, respectively (Scheme 6).

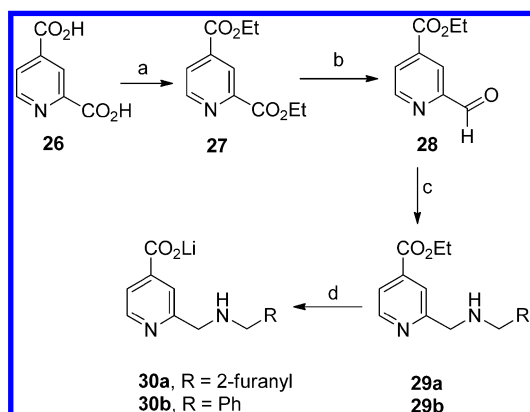
Suzuki cross-coupling reaction of 34 with trimethylboroxine afforded the C8-methyl derivative 42 which was oxidized to 4-oxo-3,4-dihydropyrido[3,4-*d*]pyrimidine-8-carbaldehyde (43);

subsequent reductive amination with the requisite primary or secondary amines gave the 8-aminomethyl derivatives 44a–g (Scheme 7, Table 5).

Compounds 52a–g (Table 6), 53a–i (Table 7), and 54a–n (Table 8) were prepared either from primary alcohol 47 by mesylate formation followed by S_N2 displacement or from carboxaldehyde 48 by reductive amination (routes A and B, respectively, Scheme 8). The pyrazole moiety at C8 of the pyrido[3,4-*d*]pyrimidin-4(3*H*)-one scaffold was introduced using an S_NAr reaction on key intermediate 35. Subsequent acidic TBS deprotection on intermediate 46 afforded the alcohol 47. Compound 59 (Table 6) bearing a longer linker at C4 of the

Scheme 3^a

^aReagents and conditions: (a) Pd(PPh₃)₄, Ag₂O, DMF, 100 °C, 1 h, 64%; (b) MeOH/H₂O, NaOH, 1 h, 46%; (c) AcOH, 48% aqueous HBr, Br₂, 0 °C to room temp for 1 h, then 75 °C for 1.5 h, 38%; (d) (i) thioacetamide, EtOH, Et₃N, reflux, 1 h, (ii) EtOH, conc HCl (2 drops), reflux, 20 min, 23%; (e) MeOH/H₂O, 1 M NaOH, room temp, 50 min, 45%.

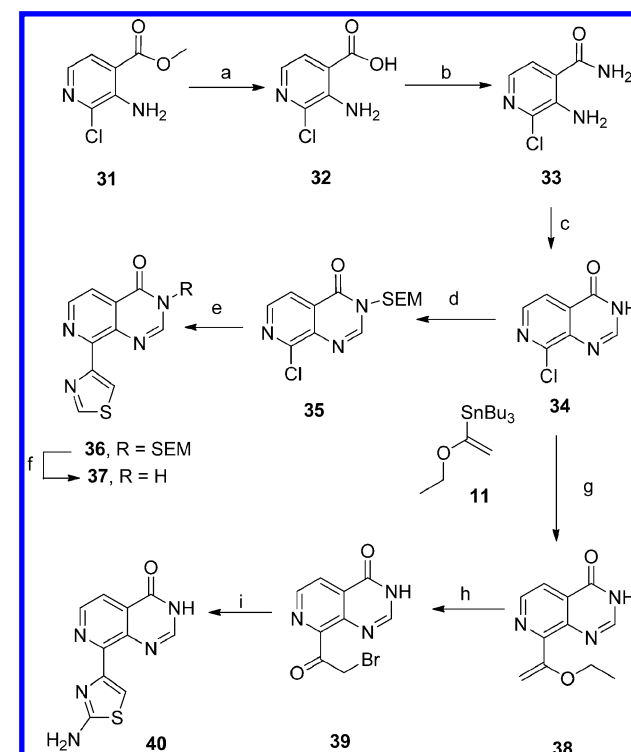
Scheme 4^a

^aReagents and conditions: (a) PTSA, EtOH, 80 °C, 79%; (b) DIBAL, THF, PhMe, -78 °C, 39%; (c) benzylamine or 2-aminomethylfuran, NaBH(OAc)₃, AcOH, CH₂Cl₂, (29a = 99%, 29b = 93%); (d) LiOH (aq), MeCN, (30a = quant, 30b = quant).

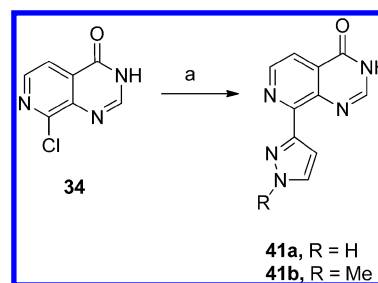
pyrazole moiety was also prepared according to route A described in Scheme 8.

RESULTS AND DISCUSSION

The discovery of chemical starting points for JmjC histone KDM inhibition was based upon an HTS campaign of a 150k compound collection tested at 30 μM versus human recombinant KDM4B (amino acid residues 1–500 with an N-terminal GST tag). The format of the HTS was the same KDM4B AlphaScreen assay described in the Methods section; this assay was also used to monitor the activity of compounds reported herein. This screening campaign provided *N*-substituted 4-(pyridin-2-yl)thiazole-2-amine derivatives exemplified by 7c as promising hits (Scheme 1, Table 1). The KDM4B inhibitory activity of 7c was confirmed with a resynthesized sample (IC₅₀ = 10.9 μM) and triggered a medicinal chemistry program to identify

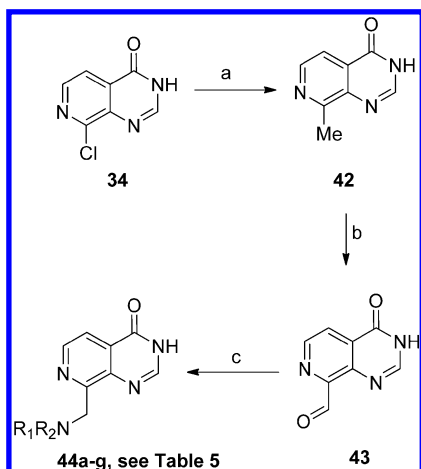
Scheme 5^a

^aReagents and conditions: (a) MeOH/H₂O, 1 M NaOH, room temp, 45 min, 77%; (b) (i) SOCl₂, DMF, reflux, 2 h, (ii) ammonium hydroxide, THF, room temp, 1.5 h, 89%; (c) CH(OEt)₃, reflux 24 h, 82%; (d) SEM-Cl, K₂CO₃, DMF, 60 °C, 4 h, 84%; (e) 4-(tributylstannyl)thiazole, Pd(PPh₃)₄, Ag₂O, DMF, 100 °C, 2 h, 32%; (f) THF, 6 M HCl, 50 °C, 4 h, 94%; (g) Pd(PPh₃)₄, 1,4-dioxane, reflux, 2 h, 64%; (h) 10% H₂O in THF, *N*-bromosuccinimide, room temp, 1 h, 72%; (i) thiourea, Et₃N, EtOH, reflux, 1 h, 13%.

Scheme 6^a

^aReagents and conditions: (a) Pd(PPh₃)₄, Na₂CO₃, DMA, ((1*H*-pyrazol-3-yl)boronic acid hydrochloride or ((*N*-methyl)pyrazol-3-yl)boronic pinacol ester, 100 °C, 1 h, (41a = 12%, 41b = 21%).

more potent, cell permeable inhibitors of the KDM4 subfamily. The methylsulfonyl analogue 7a, *p*-SO₂Et isomer 7b, and benzamido analogue 7d displayed similar KDM4 inhibitory activities to 7c (Table 1); all four analogues (7a–d) were more potent inhibitors of KDM4B relative to KDMSB by at least 3-fold under the standard assay conditions (Table 1). However, the commercially available fragment-like scaffold 4-(pyridin-2-yl)thiazol-2-amine (5) demonstrated very weak inhibition of KDM4B (30% inhibition at 100 μM) and no activity against KDMSB at 100 μM, indicating an important role for the primary amine *N*-substituent.

Scheme 7^a

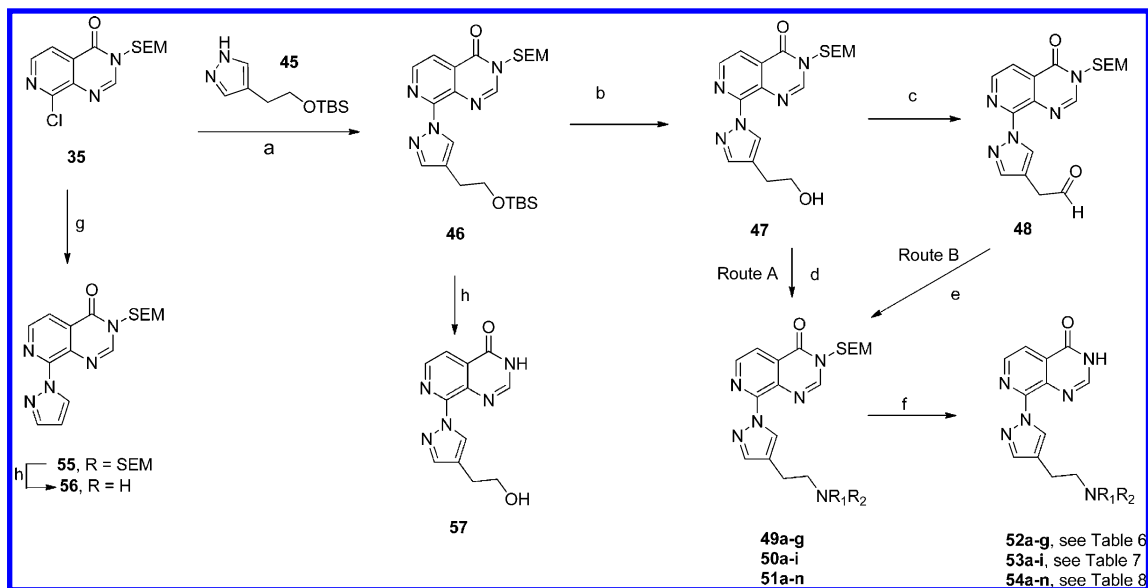
^aReagents and conditions: (a) Pd(PPh₃)₄, K₂CO₃, trimethylboroxine, DME, 90 °C, 1 h, 59%; (b) SeO₂, 1,4-dioxane, 90 °C, 8 h, 14%; (c) NaBH(OAc)₃, R₁R₂NH, MeOH/CH₂Cl₂, room temp, 1–3 h, 12–55%.

We set out to establish the binding mode of the 4-(pyridin-2-yl)thiazol-2-amine series to facilitate further medicinal chemistry design. We postulated that the pyridine nitrogen in 7a–d (Table 1) would be a major contributor to KDM4A/B binding via coordination to the metal in the JmjC-domain catalytic site analogous to the binding mode of previously reported pyridine-based KDM inhibitors such as 1–4 (Figure 1).^{24,32–34} Consistent with this notion, and also with previous reports that suggested a significant drop in potency for pyridin-3-yl regioisomers of active compounds,²⁴ the 4-(pyridin-3-yl)thiazole derivatives 8, 9a, and 9b were considerably less potent or inactive relative to their pyridin-2-yl counterparts (Tables 1 and 2).

The commercially available phenyl analogue of 5, lacking the pyridyl nitrogen (4-phenylthiazol-2-amine), was also inactive against KDM4A and KDM4B at 100 μM compound concentration (data not tabulated).

Attempts to elucidate the binding mode of 7a or close analogues by cocrystallization with KDM4A or by soaking of apo-KDM4A crystals with 7a were unsuccessful. Docking studies of the fragment-like scaffold 5 using the cocrystal structure of 2 in KDM4A (PDB code 3PDQ)³³ suggested that 5 could bind to the active site metal through bidentate coordination of the pyridyl and thiazolyl nitrogen atoms (Figure 2A,B). Furthermore, the docked pose of 5 overlaid well with the binding mode of the bipyridyl-based analogue 2-bound KDM4A cocrystal structure (PDB code 3PDQ).³³ This observation prompted the introduction of a carboxylate moiety *para* to the pyridine nitrogen in 5 to interact with K206 and Y132 (KDM4A residue numbering) in a manner analogous to that observed for the cosubstrate 2OG, NOG, and literature pyridyl-based analogues 1 and 2.^{32,33,37} Pleasingly, 15 (Table 3) demonstrated potent inhibition of KDM4A and KDM4B (IC₅₀ = 0.200 and 0.083 μM respectively, Table 3), KDM5B (IC₅₀ = 0.012 μM, Table 3) as well as KDM3A (IC₅₀ = 0.057 μM) while inhibiting KDM2A and KDM6B to a lesser extent (IC₅₀ = 1.2 and 1.0 μM, respectively). Interestingly, introduction of a carboxylate at the equivalent position *para* to the pyridine nitrogen in the *N*-(thiazol-2-yl)benzamido derivative 7d to give compound 19 (Table 3) resulted in demethylase activity similar to 7d (KDM4B IC₅₀ = 17.0 μM, Table 3) consistent with the docking predictions that binding of extended analogues at the C2 thiazole position could be compromised due to the steric clash of the benzamido substituent with the protein (Figure 2B).

Protein–ligand crystallographic analysis was mainly performed using KDM4A which has a similar JmjC catalytic site to that of KDM4B.³⁸ A crystal structure of 15 bound to KDM4A confirmed the proposed binding mode involving interactions of

Scheme 8^a

^aReagents and conditions: (a) Cs₂CO₃, anhydrous MeCN, reflux, 18 h, 71%; (b) 1 M HCl, MeOH, 0 °C, 5 min, 99%; (c) Dess–Martin periodinane, anhydrous CH₂Cl₂, room temp; (d) (i) methanesulfonic anhydride, Et₃N, anhydrous CH₂Cl₂, 0 °C, 15 min, workup, (ii) Cs₂CO₃, R₁R₂NH, anhydrous DMF, 90 °C, 15 h or Et₃N, anhydrous DMF, 50 °C, 15 h, 17–84%; (e) R₁R₂NH, anhydrous 1,2-dichloroethane, NaBH(OAc)₃, room temp, overnight, 24–69%; (f) 6 M HCl, THF, 50–60 °C, 3 to 8 h or 4 M HCl in dioxane, dioxane/H₂O, 50 °C, 16–97%; (g) pyrazole, Cs₂CO₃, anhydrous MeCN, reflux, 3 h, 80%; (h) THF, 6 M HCl, 50 °C, 4 h, (56 = 70%, 57 = 75%).

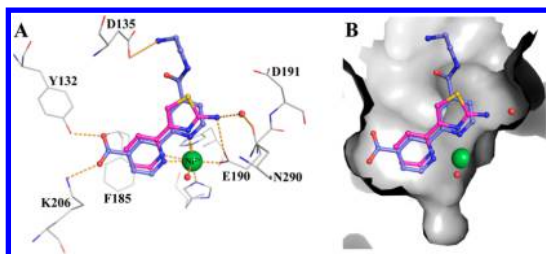


Figure 2. Overlay of a view from crystal structure of **2** (light-blue ball-and-sticks) bound to KDM4A (displayed in gray lines or gray surface; PDB code 3PDQ)³³ and a model of **5** (magenta) docked into the protein structure from 3PDQ. (A) Interaction network. (B) Surface representation. Ni(II) shown in place of the active site Fe(II).

the carboxylate moiety with K206 and Y132 and bidentate coordination of both the pyridyl and thiazolyl nitrogens to the metal. A deviation from coplanarity of the pyridyl and thiazolyl aromatic ring systems (torsional angle = 17.4°) and a rotation of the plane of the carboxylate relative to the plane of the pyridine ring was also observed (28.6°, Figure 3A). These observations are broadly consistent with the binding mode of an analogue of the triazolopyridine **3** (Figure 1)³⁴ and of aminomethyl substituted pyridines **30a**³⁶ and **30b** (Table 4). The carboxylic acid in **30b** interacts with K206 and Y132 of KDM4A and the carboxylic acid in **30a** with corresponding residues of KDM4D; furthermore, both ligands exhibit bidentate metal coordination (Figure 3D,E). The aminomethyl substituent in both **30a** and **30b** is rotated away from the plane of the biaryl ring scaffold in **15** to interact with Y175 in KDM4A and the equivalent residue in KDM4D (Y179) (Figure 3D,E); additionally, the furan oxygen of **30a** interacts with the hydroxyl moiety of Y181 in KDM4D (equivalent residue Y177 in KDM4A) (Figure 3E).

The **15**-bound KDM4A structure also revealed π -stacking of the pyridyl ring with the side chain of residue F185, an interaction of the thiazole C2-NH₂ with E190, and interaction of this exocyclic NH₂ to both D191 and N290 via a mediating water molecule (Figure 3B,C). Consistent with the latter observation, the desamino analogue **22** was a less potent KDM4 inhibitor compared to **15** (KDM4A IC₅₀ = 0.90 μ M, KDM4B IC₅₀ = 0.35 μ M; Table 3), and a further drop in potency was observed with the thiazole C2-Me analogue **25** (KDM4A IC₅₀ = 16.5 μ M, KDM4B IC₅₀ = 2.3 μ M; Table 3). Conversion of the carboxylic acid in **15** to the corresponding primary amide **16** led to a

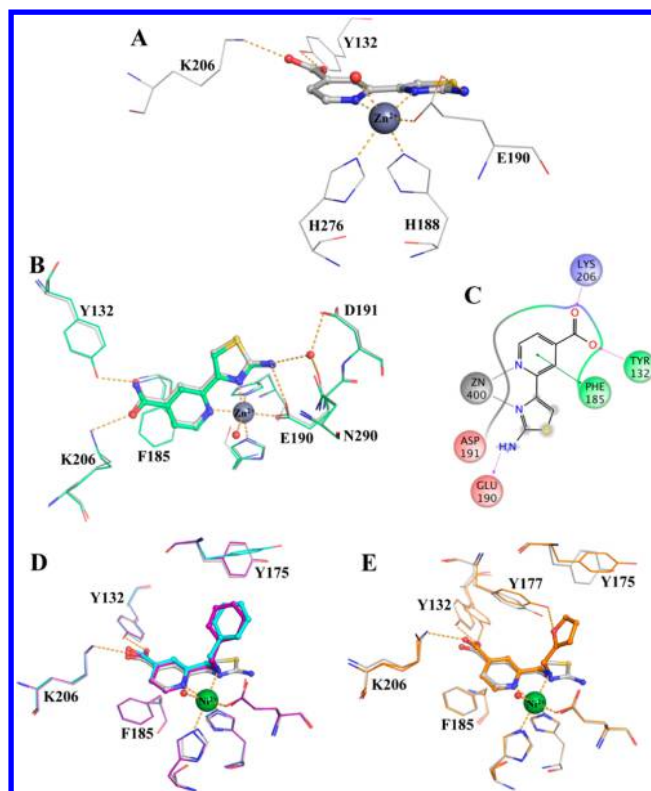


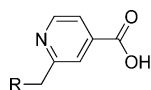
Figure 3. Views from crystal structures of **15**, **16**, and **30b** bound to KDM4A and of **30a** bound to KDM4D. (A) KDM4A-bound **15** (gray), showing a close-up view of ligand–metal coordination and interaction with Y132 and K206. (B) Overlay of KDM4A-bound **15** (gray) and **16** (green). (C) 2D interaction map of **15** with key residues in KDM4A. (D) Overlay of KDM4A-bound **15** (gray) and **30b** (purple for chain A, cyan for chain B of the asymmetric unit). (E) Overlay of KDM4A-bound **15** (gray) and KDM4D-bound **30a** (orange). Indicated residues correspond to KDM4A numbering. Zn(II) and Ni(II) are shown at the active site.

significant drop in KDM4A and KDM4B potency (500- and 400-fold, respectively), highlighting the importance of the carboxylate–K206 ionic interaction for potent histone KDM inhibition. A crystal structure of **16** bound to KDM4A showed a very similar binding mode to that of **15**. Interestingly, the primary amide of **16** and the carboxylic acid of **15** overlay well, further reinforcing the significant benefit of the carboxylate–K206

Table 3. 2-(2-Aminothiazol-4-yl)isonicotinic Acid Derivatives^b

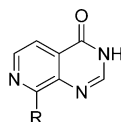
Compound	R	X	KDM4A IC ₅₀ (μ M)	KDM4B IC ₅₀ (μ M)	KDM5B IC ₅₀ (μ M)	KDM5C IC ₅₀ (μ M)
15	NH ₂	OH	0.200	0.083±0.005	0.012 ^a	0.012 ^a
16	NH ₂	NH ₂	104.2	32.7	2.2 ^a	6.8 ^a
22	H	OH	0.90	0.35±0.14	0.098	0.122
25	CH ₃	OH	16.5	2.3	1.3	1.7
19		OH	30.6	17.0	0.59	2.0

^aResults are from a single experiment. ^bResults are mean values of two independent determinations or mean (\pm SD) for $n > 2$ unless specified otherwise.

Table 4. 2-(Aminomethyl)pyridine-4-carboxylate Derivatives^b

Compound	R	KDM4A IC ₅₀ (μM)	KDM4B IC ₅₀ (μM)	KDM5B IC ₅₀ (μM)	KDM5C IC ₅₀ (μM)
30a		0.30 ^a	0.17 ^a	0.04 ^a	0.03 ^a
30b		0.95 ^a	1.2 ^a	0.13 ^a	0.06

^aResults are from a single experiment. ^bResults are mean values of two independent determinations or mean (\pm SD) for $n > 2$ unless specified otherwise. Compounds tested as their lithium salts.

Table 5. C8-Pyrido[3,4-*d*]pyrimidin-4(3*H*)-one Derivatization^b

Compound	R	KDM4A IC ₅₀ (μM)	KDM4B IC ₅₀ (μM)	KDM5B IC ₅₀ (μM)	KDM5C IC ₅₀ (μM)
58	H	1.7 \pm 0.6	1.0 \pm 0.4	1.3 ^a	2.0 ^a
40		11.5	5.0 \pm 1.2	0.124 ^a	0.331 ^a
37		8.0 \pm 3.6	3.1 \pm 1.1	0.31	0.83
34	Cl	No activity at 100μM ^a	30% at 200μM ^a	32% at 100μM ^a	22% at 100μM ^a
41a		6.9	2.8	4.1	7.3
41b		42.8	9.2	21.4	103.4
56		16.7 ^a	4.6	7.0 ^a	9.4 ^a
44a		15.6	6.5	0.69	0.44
44b		6.1	3.1	0.63	0.73
44c		13.1	8.5	1.4	1.3
44d		9.8 ^a	7.8 ^a	7.0	8.4
44e		>100	>100	66.0	111.0
44f		>100	81.5	3.9	>100
44g		58.6	24.6	2.0	88.0 ^a

^aResults are from a single experiment. ^bResults are mean values of two independent determinations or mean (\pm SD) for $n > 2$ unless specified otherwise.

charge interaction (Figure 3B). Although the ionizable carboxylic acid appeared beneficial for ligand affinity, we considered it a significant contributing factor to the observed poor cellular permeability for **15** (Caco-2 A to B flux $<0.8 \times 10^{-6}$ cm/s). Therefore, we focused on pyridine-4-carboxylic acid isosteres with the potential to coordinate to the active site metal, make strong interactions with K206/Y132 (KDM4A) and to be only partially ionized at physiological pH to improve cellular permeability while maintaining potent enzyme binding. Our attention was drawn to the pyrido[3,4-*d*]pyrimidin-4(3*H*)-one scaffold (**58**, Table 5, Figure 4) kindly disclosed to us by GSK³⁹

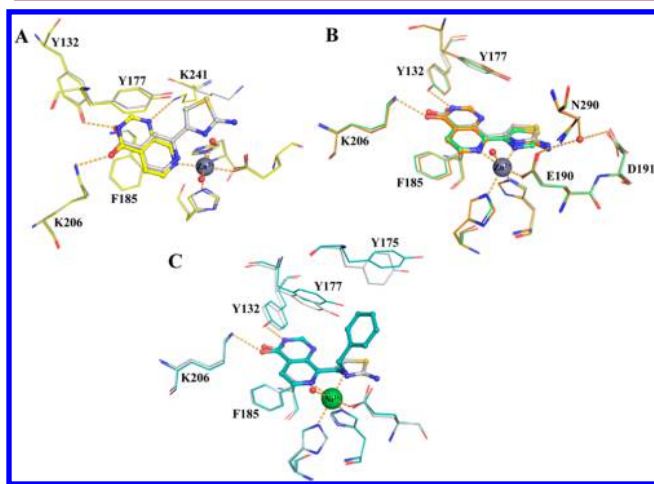


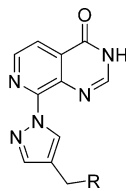
Figure 4. Comparison of binding modes of **15**, **37**, **40**, and **58** to KDM4A and **44a** bound to KDM4D. (A) Overlay of KDM4A-bound **15** (gray) and **58** (yellow). (B) Overlay of KDM4A-bound **15** (gray), **37** (light-green), and **40** (orange). (C) Overlay of KDM4A-bound **15** (gray) and KDM4D-bound **44a** (light blue). The indicated residue numbers correspond to KDM4A numbering. Zn(II) and Ni(II) are shown in place of the active site Fe(II).

and also reported in the patent literature as a template for JmjC KDM inhibition.⁴⁰ The bicyclic aromatic scaffold **58** is a highly efficient ligand for both KDM4 and KDM5 subfamily members (KDM4B $IC_{50} = 1.0 \mu\text{M}$, $LE = 0.76$, and KDM5B $IC_{50} = 1.3 \mu\text{M}$, $LE = 0.75$; Table 5) while a less potent inhibitor of KDM3A ($IC_{50} = 26.2 \mu\text{M}$), KDM2A (29% inhibition at $100 \mu\text{M}$), and KDM6B (28% inhibition at $100 \mu\text{M}$). Pleasingly, **58** also displayed high cellular permeability (Caco-2 A to B flux $= 42.61 \times 10^{-6}$ cm/s) with a measured pK_a for the pyridopyrimidinone amide moiety of 8.23.⁴¹

The **58**-bound KDM4A structure demonstrates simultaneous coordination of the pyrido[3,4-*d*]pyrimidin-4(3*H*)-one scaffold to the active site metal via the pyridine nitrogen (position 7) and interaction of the pyrimidinone CONH moiety with K206/Y132; in addition, N1 of **58** is positioned to interact with the side chain of K241. This network of interactions is consistent with the highly ligand efficient inhibition profile of **58** versus KDM4A and KDM4B, which are very similar in their JmjC catalytic sites. Superposition of the **15**-bound and **58**-bound KDM4A structures (Figure 4A) suggested that the pyrido[3,4-*d*]pyrimidin-4(3*H*)-one scaffold **58** may provide a suitable replacement for the pyridine-4-carboxylate, whereby derivatization at the C8 position of **58** could lead to bidentate metal coordination and access to the histone peptide binding site (vide infra). To test this hypothesis, the hybrid structures **37** and **40** were synthesized (Scheme 5, Table 5). Compound **40** displayed lower KDM4B inhibitory activity ($IC_{50} = 5.0 \mu\text{M}$, Table 5)

compared to **15** and **58**. A similar trend was observed with the 2-desamino analogue **37** (KDM4B $IC_{50} = 3.1 \mu\text{M}$, Table 5). Compound **37** proved a more potent inhibitor of KDM3A ($IC_{50} = 0.89 \mu\text{M}$) and KDM5B ($IC_{50} = 0.31 \mu\text{M}$; Table 5) and showed weaker inhibition of KDM2A (59% inhibition at $100 \mu\text{M}$) and KDM6B (31% inhibition at $100 \mu\text{M}$), consistent with the profile of compound **15**. Crystal structures of **40** and **37** bound to KDM4A show bidentate coordination to the metal as well as the predicted interactions with K206/Y132 (Figure 4B). However, interaction of K241 with N1 of the pyridopyrimidinone scaffold is no longer observed for C8-substituted pyridopyrimidinones **37** and **40**, which may contribute to their lower potency compared to **58** (Figure 4A,B). We postulate that steric bulk of the thiazole C8 substituent in **37** and **40** hinders interaction of the scaffold with K241. Furthermore, we note that metal coordination of the thiazole nitrogen in **37** and **40** may result in suboptimal interactions of the pyridopyrimidinone CONH moiety with K206/Y132 owing to the planar bicyclic scaffold which precludes the 28.6° dihedral angle between the pyridine and carboxylate observed in our **15**-bound KDM4A structure (Figures 3A, 4A,B). Interestingly, the torsion angles between the planes of the pyridopyrimidinone and the thiazole ring systems in **37** and **40** are similar to that observed between the pyridine and the thiazole in **15** (4.7° and 7.2° difference with respect to **15**, respectively), rendering the metal-coordination geometry similar for **15**, **37**, and **40** (Figure 4B). Although introduction of a C8-thiazole substituent led to a slight decrease in KDM4A and KDM4B potency compared to **58**, we envisaged that potency for this class of compounds could be improved by introducing favorable interactions with D135 and other residues in the histone peptide binding site, a tactic previously reported to yield potent JmjC histone demethylase modulators in the bipyridyl scaffold exemplified by **2** (Figure 2A).³³ Access to the histone peptide binding pocket required derivatization through a position equivalent to the sulfur atom in **37** (see Figures 2A,B and 4A,B) and necessitated the introduction of alternative heterocyclic rings at the C8 position of the pyrido[3,4-*d*]pyrimidin-4(3*H*)-one scaffold (Table 5).

We introduced a variety of five-membered heterocycles at C8 of the pyrido[3,4-*d*]pyrimidin-4(3*H*)-one scaffold **58**, including pyrazol-3-yl and pyrazol-1-yl moieties (**41a** and **56**, respectively, Table 5) which exhibited similar potency versus KDM4B and KDM5B. We also investigated whether methylamino substituents at C8 could provide access to the pocket occupied by the trimethylated lysine of the H3K9Me₃ peptide substrate, as previously described for **30a** and **30b** in the pyridine-4-carboxylic acid series (Table 4; Figure 3D,E). Compounds **44a** and **44b** were both less potent inhibitors of KDM4B and KDM5B compared to their pyridine-4-carboxylate counterparts **30b** and **30a**, respectively (Tables 4, 5). We confirmed the binding mode of **44a** to KDM4D by cocrystal structure determination, which proved consistent with that of the parent compound (compare Figure 3D,E and Figure 4C). Interestingly, both aminomethyl-substituted pyridopyrimidinones **44a** and **44b** display a preference for KDM5B/C inhibition over KDM4A/B. Tertiary amine analogues **44c–g** were designed to rescue KDM4 potency by maintaining bidentate metal chelation while also extending into space occupied by the C8-thiazole of **37** or **40** and benefiting from interactions with Y175 and Y177 in KDM4A (Figure 4). At best, the tertiary aminomethyl compounds were comparable in potency to simple C8-heterocyclic substituted derivatives **41a,b** and **56** (Table 5). Considering the data presented in Table 5, and cognizant of synthetic tractability, we focused our

Table 6. 8-(1*H*-Pyrazol-1-yl)pyrido[3,4-*d*]pyrimidin-4(3*H*)-one Derivatives^b

Compound	R	KDM4A IC ₅₀ (μM)	KDM4B IC ₅₀ (μM)	KDM5B IC ₅₀ (μM)	KDM5C IC ₅₀ (μM)	Caco-2 (x10 ⁻⁶ cm/s)
57		21.8	8.8	4.6 ^a	8.4 ^a	0.76
52a		4.1±3.7	2.3	0.35	0.34	0.76
52b		1.4	0.75	0.071	0.150	3.08
52c		1.8	0.65	0.199	0.342	1.64
52d		0.90±0.59	0.39±0.12	0.042	0.078	9.98
52e		0.39	0.165	0.048	0.080	21.21
52f		0.66	0.40	0.072	0.136	0.76
52g		0.60	0.34	0.048	0.076	n.d.
59		0.88	0.26	0.048	0.064	n.d.

^aResults from a single experiment. n.d. = not determined ^bResults (IC₅₀s) are mean values of two independent determinations or mean (±SD) for *n* > 2 unless specified otherwise.

effort on elaboration of the pyrazol-1-yl analogue **56** by targeting residues in the histone substrate binding site including D135 (KDM4A) (Table 6).

Substitution at the pyrazole-C4 position with a hydroxyethyl group (**57**) was tolerated and resulted in a similar KDM4/5 inhibitory profile to **56** (Tables 5 and 6). Introduction of a basic nitrogen at the pyrazole-C4 substituent, exemplified by compounds **52a**, **52b**, and **52c**, resulted in at least a 4-fold improvement in KDM4A/B inhibitory activity (Table 6); notably, all three compounds were more potent inhibitors of KDM5B/C compared to KDM4A/B. Introduction of a *p*-fluorobenzyl group (**52d**), gave a more potent inhibitor of KDM4B, KDM5B, and KDM5C (IC₅₀ = 0.39, 0.042, and 0.078 μM, respectively, Table 6). Pleasingly, **52d** displayed a weaker inhibitory activity against KDM2A (IC₅₀ = 13.4 μM), KDM3A (IC₅₀ = 13.9 μM), and KDM6B (IC₅₀ = 26.3 μM) relative to KDM4/5 subfamily members. A crystal structure of **52d** bound to KDM4A revealed

that the compound bound in multiple conformations, with the two most predominant binding modes depicted in Figure 5. In conformation A, the pyrazole-C4 substituent adopts an extended conformation with the *p*-fluorobenzyl group oriented toward the solvent accessible area; this induces movement of the side chain of Y175 and displaces the nearby loop (residues 165–175). However, no interaction between **52d** and the induced side chain conformation of Y175 is observed (minimal distance of 4.7 Å between a carbon of the Y175 aromatic ring and a carbon of the *p*-fluorophenyl group of **52d**). In conformation B, the *p*-fluorobenzyl group of the pyrazole-C4 substituent oriented toward an asparagine/glutamine-rich pocket (residues 73, 84, and 86, Figure 5). In conformation B, the basic nitrogen of the pyrazole-C4 substituent is proximal to D135 with a minimum interaction distance of 2.9 Å (distances between 2.9 and 3.2 Å depending upon the chain in the asymmetric unit), slightly shorter compared with the equivalent distance in conformation A

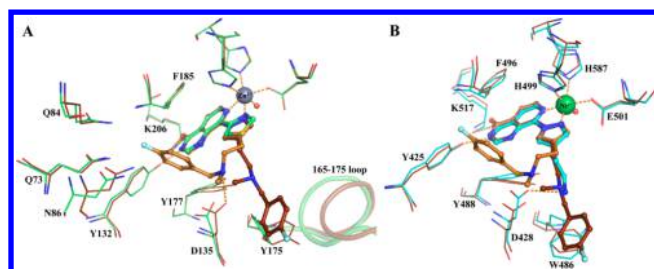


Figure 5. (A) Overlay of views from crystal structure of KDM4A-37 (light-green) and -52d (two main conformations: dark-brown for conformation A and light-brown for conformation B). (B) Overlay of 52d bound to KDM4A (brown) and KDM5B (cyan), the indicated residue numbers correspond to KDM5B numbering. Zn (II) or Ni(II) are shown in place of the active site Fe (II).

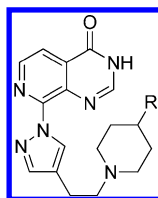
(3.4–4.3 Å). Attempts to cocrystallize compounds presented in this study with KDM5B proved more challenging relative to KDM4A crystallography; however, we were successful in resolving a crystal structure of 52d bound to KDM5B (Figure 5B), which shows coordination of both the pyridyl and pyrazole N2 nitrogen to the active site metal and interaction of the pyridopyrimidinone CONH moiety with K517/Y425 (equivalent to residues K206/Y132 in KDM4A). The electron density of the *p*-fluorobenzyl group in this crystal structure was poor, precluding accurate positioning of this moiety. However, the binding mode of the well-defined ligand scaffold to KDM5B was similar to that observed in the structure of 52d bound to KDM4A.

Pleasingly, 52d displayed cellular permeability (Caco-2 A to B flux = 9.98×10^{-6} cm/s, Table 6) and moderate HLM and MLM stability (40% and 42% metabolized after a 30 min incubation, respectively). Surprisingly, we found that 52d had high in vivo plasma clearance (iv clearance in mouse of 1640 mL/min/kg, following a 6 mg/kg iv compound administration), which we suspected may be due to aldehyde oxidase (AO)-mediated metabolism.⁴² We subsequently identified the C2 position of the pyrido[3,4-*d*]pyrimidin-4(3*H*)-one template as the major site of AO-mediated metabolism.⁴³

The 3,4-dichlorobenzyl analogue 52e also demonstrated cellular permeability (Caco-2 A to B flux = 21.21×10^{-6} cm/s, Table 6); however, attempts to gain additional KDM4A/B affinity by introduction of hydrogen bond interactions with N86, Q73, or Q84 (52f and 52g; Figure 5) were unsuccessful (Table 6). Homologation of the pyrazole-C4 substituent by one methylene unit (59) also failed to improve KDM4A or KDM4B inhibition (Table 6).

The multiple ligand conformations observed in the 52d-bound KDM4A structure suggested that no single binding mode was favored and is consistent with multiple degrees of freedom in the ligand conformation. Thus, we next attempted to constrain the pyrazole-C4 substituent by introduction of a piperidine ring. This approach led to the synthesis of 53a, a potent and cell permeable (Caco-2 A to B flux = 6.86×10^{-6} cm/s) KDM4A and KDM4B inhibitor (IC_{50} = 0.126 and 0.050 μ M, respectively) which also strongly inhibited KDM5B and KDM5C (IC_{50} = 0.014 and 0.023 μ M, respectively; Table 7). This KDM4 and KDM5 subfamily profile differentiates 53a from 52d, which is

Table 7. C8-Pyrido[3,4-*d*]pyrimidin-4(3*H*)-one Derivatization^a



Compound	R	KDM4A IC_{50} (μ M)	KDM4B IC_{50} (μ M)	KDM5B IC_{50} (μ M)	KDM5C IC_{50} (μ M)
53a		0.126	0.050	0.014	0.023
53b		0.181	0.118	0.021	0.041
53c		0.147	0.079	0.017	0.021
53d		0.158	0.062	0.015	0.022
53e		0.144	0.068	0.015	0.023
53f		0.54	0.149	0.028	0.041
53g		0.136	0.072	0.016	0.021
53h		0.60	0.207	0.026	0.050
53i		0.77	0.247	0.043	0.057

^aResults (IC_{50} s) are mean values of two independent determinations unless specified otherwise.

approximately 9-fold more potent in inhibiting KDM5B compared to KDM4B (Table 6). Pleasingly, **53a** maintained selectivity for KDM4 and KDM5 subfamily inhibition versus KDM2A ($IC_{50} = 8.6 \mu M$), KDM3A ($IC_{50} = 4.8 \mu M$), and KDM6B ($IC_{50} = 48.5 \mu M$). The crystal structure of **53a** bound to KDM4A confirmed a single binding mode in which the ligand extends toward the histone peptide binding site similar to conformation A of **52d** (Figures 5 and 6). The bulky pyrazole-C4 substituent of **53a** induces movement of the Y175 side chain and the nearby loop (residues 165–175) as observed in conformation A of **52d**. We also observed a hydrophobic interaction between the piperidine ring of **53a** with the side chain of Y175 (3.5 Å between proximal piperidine carbon atoms and the aromatic ring of Y175, Figure 6). Notably, the distance between the piperidine nitrogen and the carboxylate of D135 is 4 Å, longer than the equivalent distance observed in a crystal structure of **52d** (conformation B) bound to KDM4A (Figures 5 and 6).

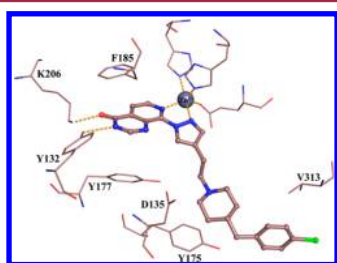


Figure 6. Binding mode of **53a** in KDM4A. Zn(II) is shown in place of the active site Fe(II).

Additionally, the *p*-chlorobenzyl group points toward the histone peptide binding site and the solvent accessible area creating a new hydrophobic interaction with V313 (3.9 Å between the *p*-chlorobenzyl of **53a** and the nearest side chain carbon of V313).

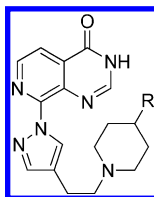
Considering these structural observations, including the single observed conformation of the pyrazole-C4 substituent in **53a**, we further explored the hydrophobic interactions with V313 (Table 7). Replacement of *p*-Cl with H (**53b**), F (**53c**), CF₃ (**53d**), or introduction of an additional *meta* substituent (**53e** and **53g**) resulted in a KDM4A/B and KDM5B/C inhibitory profile broadly similar to that of **53a** (Table 7). The *m*-methoxybenzyl analogue (**53f**) was a less potent inhibitor of KDM4A relative to **53a** although KDM5B/C potency was maintained (Table 7). Replacement of the *p*-chlorophenyl in **53a** with heterocyclic moieties failed to improve KDM4A/B or KDM5B/C inhibitory activities (compounds **53h** and **53i**, Table 7).

In a further attempt to restrain conformational freedom in the pyrazole side chain of **53a**, we attached the *p*-chlorophenyl moiety directly to the piperidine 4 position (**54a**); this tactic broadly maintained KDM4A/B and KDM5B/C inhibitory activities (KDM4B $IC_{50} = 0.086 \mu M$, KDM5B $IC_{50} = 0.030 \mu M$; Table 8). Notably, **54a** demonstrated selectivity for KDM4B and KDM5B versus KDM2A ($IC_{50} = 6.74 \mu M$) and also displayed cellular permeability (Caco-2 A to B flux = 2.66×10^{-6} cm/s, Table 8). Replacement of the *p*-Cl substituent in **54a** with F (**54b**), OMe (**54c**), SO₂Me (**54d**), or CN (**54e**) resulted in a similar KDM4A/B inhibitory profile to that of **54a**. Interestingly, balanced inhibition of KDM4 and KDM5 subfamily members was observed for **54a**, **54b**, and **54c** (Table 8). Analogue **54f** bearing an *o*-chlorophenyl substituent and the unsubstituted phenyl derivative **54g** exhibited weaker KDM4A and KDM4B inhibition compared to that of **54a** (Table 8). Heterocyclic replacements for the *p*-chlorophenyl moiety in **54a** gave a similar

KDM4A/B and KDM5B/C inhibition profile (see **54h** and **54i**, Table 8). The thiophene derivative (**54i**) was a less potent inhibitor of KDM3A ($IC_{50} = 8.3 \mu M$), KDM6B (25% inhibition at 100 μM), and KDM2A ($IC_{50} = 2.4 \mu M$). Moderate HLM and MLM stability was observed for **54i** (49% and 62% metabolized after a 30 min incubation, respectively), and cellular permeability was maintained (Caco-2 A to B flux = 17.83×10^{-6} cm/s). Notably, introduction of a 3,5-dichlorophenyl, compound **54j** gave the most potent inhibitor of KDM4 and KDM5 subfamily members in this series, with KDM4A/B and KDM5B/C potencies indicating a balanced inhibition profile (KDM4A/B $IC_{50} = 0.080$ and $0.017 \mu M$, KDM5B/C $IC_{50} = 0.014$ and $0.051 \mu M$, respectively, Table 8). Pleasingly, **54j** showed cellular permeability (Caco-2 A to B flux = 6.34×10^{-6} cm/s) and a selective inhibition profile versus KDM3A ($IC_{50} = 6.1 \mu M$), KDM6B (4% inhibition at 100 μM), and KDM2A ($IC_{50} = 2.4 \mu M$). The *m*-Cl analogue **54k** displayed a similar profile to that of **54j** (Table 8) and benefited from low MLM and HLM turnover (13% and 17% metabolized respectively after a 30 min incubation). Compound **54k** also displayed a selective inhibition profile versus KDM2A ($IC_{50} = 12.9 \mu M$), KDM3A ($IC_{50} = 5.3 \mu M$), and KDM6B (15% inhibition at 100 μM). Furthermore, profiling of **54k** in a 50-kinase panel, representative of the human kinome,⁴⁴ at a concentration of 1 μM revealed no significant kinase inhibitory activity (Supporting Information, Table S2). Analogues **54l**–**n** also demonstrated a broadly balanced KDM4B and KDM5B inhibition profile and showed good cellular permeability in the Caco-2 assay, reinforcing the SAR trend in this 4-phenyl piperidine subseries (Table 8).

Cellular activity of **54k** was assessed in HeLa cells transiently overexpressing wild-type (WT) KDM4A or KDM5B or the respective mutants (MUT) lacking catalytic activity. Cells were treated with the inhibitor, and changes in the global methylation levels were quantified by high content immunofluorescence assay after 24 h.⁴⁵ Global hypomethylation was observed in cells overexpressing either WT KDM4A or WT KDM5B as determined by reduction in the levels of methyl-lysine antibody staining (relative to cells overexpressing the corresponding MUT demethylase or nontransfected cells). Treatment with **54k** resulted in a concentration-dependent increase of the respective methyl mark (H3K9Me₃ for KDM4A, H3K4Me₃ for KDM5B) in cells overexpressing WT demethylase. At high concentrations of **54k** (>50 μM), H3K9Me₃ levels approached those in HeLa cells overexpressing MUT KDM4A, consistent with cell-based inhibition of KDM4A demethylase activity; similarly, at high concentrations of **54k**, H3K4Me₃ levels approached those in HeLa cells overexpressing MUT KDM5B, consistent with cell-based inhibition of KDM5B demethylase activity. Occasionally, at the highest concentrations, an effect on the methylation mark was also observed in cells overexpressing MUT KDM, pointing to inhibition of either the endogenous enzyme(s) or an unspecific effect (Supporting Information, Figure S1).

In studies to assess the quality of promising analogues as potential lead compounds, we noted chemical instability of **54j** and **54l** when left in air at room temperature for prolonged periods; mass spectrometry analysis suggested an oxidation-mediated degradation. However, compound **54j** was stable for >8 weeks as solution in DMSO when stored under a nitrogen atmosphere. These observations prompted us to resynthesize **54j** and study its stability as a solution in DMSO kept at room temperature with no protection from air and also in solid form kept at room temperature under a nitrogen atmosphere. LCMS and NMR (solid sample) monitoring indicated no degradation for up to 8 weeks. Given these observations, we recommend that,

Table 8. C8-Pyrido[3,4-*d*]pyrimidin-4(3*H*)-one Modifications^b

Compound	R	KDM4A IC ₅₀ (μM)	KDM4B IC ₅₀ (μM)	KDM5B IC ₅₀ (μM)	KDM5C IC ₅₀ (μM)	Caco-2 (x10 ⁻⁶ cm/s)
54a		0.138	0.086±0.019	0.030 ^a	0.067 ^a	2.66
54b		0.175	0.061	0.018	0.052	14.33
54c		0.123	0.039±0.002	0.010 ^a	0.034 ^a	5.77
54d		0.109	0.069	0.010	0.032	n.d.
54e		0.118	0.069	0.007 ^a	0.024 ^a	1.84
54f		0.411	0.179	0.056	0.119	n.d.
54g		0.456	0.274	0.058 ^a	0.142 ^a	8.05
54h		0.145	0.055	0.015	0.050	1.14
54i		0.143	0.029	0.026	0.046	17.83
54j		0.080±0.042	0.017±0.002	0.014	0.051	6.34
54k		0.102±0.058	0.031±0.012	0.023	0.065	11.80
54l		0.138	0.041	0.043 ^a	0.126 ^a	21.21
54m		0.110	0.036	0.011 ^a	0.054 ^a	15.74
54n		0.128	0.039	0.018 ^a	0.070 ^a	15.31

^aResults are from a single determination. n.d. = not determined ^bResults (IC₅₀s) are mean values of two independent determinations or mean (±SD) for *n* > 2 unless specified otherwise.

as a precaution, compounds of this class are stored under a nitrogen atmosphere.

Crystal structures of **54a** and **54j** bound to KDM4A showed that both compounds adopt an extended conformation consistent with that observed for **52d** and **53a** (Figure 7A). The orientation and position of the piperidine ring in **54a** and **54j** is perpendicular to the aromatic ring of Y175 in KDM4A and is rotated by nearly 90° compared to the piperidine ring of **53a** (compare Figures 6 and 7A). The piperidine ring in **54a** or **54j** maintains hydrophobic interactions with the side chain of Y175 (distances of 3.5 and 3.1 Å between the nearest carbon atom of the piperidine and the aromatic ring of Y175 for **54a** and **54j**,

respectively). However, in the **54a**- and **54j**-bound structures, the piperidine nitrogen resides at a minimum distance of 3.9 and 3.8 Å from the carboxylate of D135, respectively, which is longer than the equivalent distance in the **52d**-KDM4A complex (conformation B). Notably, the *p*-chlorophenyl and *m*-dichlorophenyl groups of **54a** and **54j** both engage in hydrophobic interactions with V313 of KDM4A, albeit with a slightly different orientation of the aromatic ring (Figure 7). We observe a closer interaction of one *m*-Cl of **54j** with the side chain of V313 (distance of 3.5 Å, Figure 7B) compared to the aromatic ring of **54a** (distance of 4 Å), potentially explaining the enhanced KDM4A/B inhibition of **54j**; indeed, this hydrophobic V313

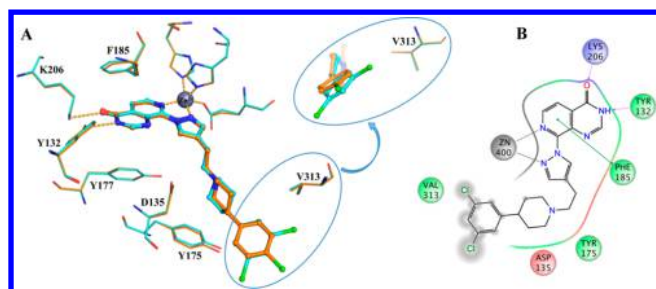


Figure 7. (A) Overlay of KDM4A-bound **54a** (orange) and **54j** (cyan). (B) 2D interaction diagram of **54j** showing interactions with key residues in KDM4A. Zn(II) is shown for the active site Fe(II).

interaction may contribute to the balanced KDM4 and KDM5 activity profile of these compounds through enhancing KDM4 subfamily affinity.

CONCLUSION

An HTS campaign versus the JmjC histone lysine demethylase KDM4B resulted in the discovery of *N*-substituted 4-(pyridin-2-yl)thiazole-2-amine derivatives as promising hit compounds. Comparison with previously reported pyridine-based JmjC KDM inhibitors generated a binding mode hypothesis, and subsequent incorporation of an appropriately positioned carboxylic acid moiety led to the discovery of **15**, a potent inhibitor of the KDM3, KDM4, and KDM5 KDM subfamilies but which lacked cellular permeability. A crystal structure of **15** bound to KDM4A confirmed the proposed binding mode involving interactions of the carboxylate moiety with K206 and Y132 as well as bidentate coordination of both the pyridyl and thiazolyl nitrogens to the active site metal. Interestingly, the corresponding primary amide **16** maintained this binding mode; however, loss of the carboxylate–K206 interaction led to a >400-fold reduction in potency, illustrating the dominance of this ionic interaction in the buried KDM4 catalytic site. Replacement of the pyridine-4-carboxylate scaffold in **15** with the less acidic, bicyclic pyrido[3,4-*d*]pyrimidin-4(3*H*)-one isostere **58** ($pK_a = 8.23$) gave cell-permeable KDM inhibitors with maintained affinity, presumably due to ionization of the weakly acidic scaffold in the KDM4 active site. A crystal structure of **58** bound to KDM4A demonstrated simultaneous coordination to the active site metal via the pyridine nitrogen, interaction with K206/Y132 via the pyrimidinone CONH moiety, and interaction with the side chain of K241 through *N*1 of the scaffold. Subsequent structure-guided optimization at C8 of the pyrido[3,4-*d*]pyrimidin-4(3*H*)-one allowed extension into the histone peptide binding site by virtue of a C8-pyrazole moiety. This tactic favored bidentate coordination to the active site metal through both the pyridine and pyrazole *N*2 nitrogen as well as concomitant additional pyrazole substitution to gain beneficial interactions with D135 and Y175 (KDM4A residue numbering) as exemplified by a crystal structure of **52d** bound in KDM4A. However, this **52d**-bound crystal structure also revealed alternative bound conformations of the flexible pyrazole C4 substituent, suggesting that conformational restriction may be required to further benefit from interactions in the histone peptide binding site. Incorporation of a rigidifying piperidine linker into pyrazole C4 substituent and subsequent positioning of a *meta*-substituted phenyl ring at the piperidine 4-position, resulted in the discovery of potent JmjC histone demethylase inhibitors such as **54j**, **54k**, and **54i**. A crystal structure of **54j** bound in KDM4A demonstrates a conserved bidentate binding mode of the

C8-pyrazolo-pyrido[3,4-*d*]pyrimidin-4(3*H*)-one scaffold to the active site metal and additional beneficial interactions of the 4-phenylpiperidine substituent with D135 and Y175 as well as a further hydrophobic interaction with V313 of KDM4A (KDM4A residue numbering), which we postulate is important to the balanced KDM4 and KDM5 activity profile of these compounds. Importantly, incorporation of the conformationally constrained 4-phenylpiperidine in derivatives **54j** and **54k** results in selective inhibition of the KDM4 and KDM5 subfamily demethylases over representative exemplars of the KDM2, KDM3, and KDM6 subfamilies, cellular permeability in the Caco-2 assay, and, for **54k**, we demonstrate inhibition of H3K9Me₃ and H3K4Me₃ demethylation in a cell-based assay. We propose that compounds such as **54k** could be utilized for the study of KDM4/KDM5 subfamilies in a cellular context. As both KDM4 and KDM5 family members have been implicated in breast, prostate, and other cancer contexts, such tool compounds may be particularly useful in studying the merits of dual inhibition of these family members in cell-based assays. In addition, the SARs and the ligand–protein interactions presented in this study could provide valuable leads for the further exploring the design and synthesis of KDM4 or KDM5 subfamily selective compounds with which to elucidate the role of the JmjC catalytic domain activity of these subfamilies in human disease. We are continuing our research toward the identification of potent, cell permeable, and selective inhibitors of the KDM4 subfamily with which to study the role of KDM4 enzyme function in cancer biology and to further explore the potential of such compounds as anticancer agents. We will report this work in future communications.

EXPERIMENTAL SECTION

KDM4A and KDM4B AlphaScreen Biochemical Assays. Protein production and purification: Baculovirus containing residues 1–500 of KDM4B with an N-terminal GST tag were generated according to Bac-to-Bac protocol. Following infection of *Sf9* insect cells, protein was purified by GSH affinity chromatography followed by gel filtration (Superdex 200). Purification of KDM4A is described in the crystallography section. For the purpose of biochemical assays, the His tag was not removed.

Enzyme activity was measured using an AlphaScreen assay that monitored the demethylation of a biotinylated trimethylated H3K9 peptide using a H3K9 dimethyl specific antibody and appropriate donor and acceptors beads from PerkinElmer Life Sciences.⁴⁶ For each compound, a 10 mM stock concentration in 100% DMSO was used. Compounds were dispensed using an ECHO 550 acoustic dispenser (Labcyte Inc., Sunnyvale, CA, USA) to generate 8 pt dilution curves directly into 384-well Proxiplates (no. 6008289, PerkinElmer, Waltham, MA, USA) to give final assay concentrations in the range 0.0005–100 μ M in 2% (v/v) DMSO as appropriate. The enzyme reaction was performed in assay buffer which consisted of HEPES (50 mM, pH 7.5), BSA (0.1% w/v), sodium ascorbate (100 μ M), 2OG (2 μ M for KDM4B or 10 μ M for KDM4A), ammonium iron(II) sulfate hexahydrate (1 μ M), and Tween 20 (0.01% v/v). Compounds were preincubated for 10 min with 2.5 μ L enzyme N-terminal GST KDM4B prepared in-house (0.5 nM final concentration) or His tagged KDM4A prepared in-house (1.5 nM final concentration) before the addition of 2.5 μ L of peptide (ARTKQTARK(Me₃)STGGKAPRKQLA-GGK-biotin, Genecust, 30 nM final concentration). The plate was sealed and centrifuged at 1000 rpm for 1 min before being left for 20 min at room temperature. The reaction was stopped with the addition of 2.5 μ L of EDTA (30 mM final concentration) before the addition of 2.5 μ L of AlphaScreen detection reagents (no. 6760606M, PerkinElmer) and antibody. The detection reagents containing IgG mouse acceptor beads, streptavidin donor beads (20 μ g/mL final concentration), and an antidimethyl H3K9 antibody (no. Ab1220, 0.5 nM final concentration) were preincubated for 1 h in detection buffer containing HEPES

(50 mM, pH 7.5), BSA (0.1% w/v), and Tween 20 (0.01% v/v) prior to addition to the plate. Plates were incubated at room temperature for 1 h in the dark before being read on an EnVision multilabel reader (PerkinElmer Life Sciences), using an AlphaScreen format. The signal was expressed in counts per second. All data analysis was carried out using the Studies package from Dotmatics (Bishops Cleeve, UK). The percentage inhibition was calculated relative to blank wells (containing no enzyme and 2% DMSO) and total wells (containing all reagents and 2% DMSO). IC₅₀s were generated using a four-parameter logistics fit.

KDM5B and KDM5C AlphaScreen Biochemical Assays. All buffer components were from Sigma-Aldrich unless otherwise stated and were of the highest purity available. Bovine serum albumin fraction V was essentially free from fatty acids and globulins (Sigma-Aldrich, code A7030). 2-[4-(2-Hydroxyethyl)piperazin-1-yl]ethanesulfonic acid (HEPES) buffer was from Life Technologies (code BI8181). The biotinylated peptide ligand substrate used for the KDM5 assay (H3(1–21)K4-Me₃-GGK Biotin) was from Anaspec (code 64192). Anti H3K4Me₂ antibody was from Cell Signaling Technology (code 9725S), and AlphaScreen General IgG detection kit was from PerkinElmer. AlphaScreen assay buffer (50 mM HEPES pH 7.5, 0.1% BSA, 0.01% Tween-20) was prepared fresh each week, filter sterilized through a 0.2 μm filter, and stored at 4 °C. Ferrous ammonium sulfate (FAS) was dissolved fresh each day to 400 mM (156.856 mg/mL) in 20 mM HCl and diluted to 1 mM in deionized water. 2OG was prepared fresh each day by dissolving to 10 mM (1.901 mg/mL) in deionized water. L-Ascorbic acid (L-AA) was dissolved to 50 mM (8.806 mg/mL) in deionized water. Compound dispensing was performed using an ECHO-550 acoustic dispenser (Labcyte), and all reagent dispenses were performed using a multidrop combi reagent dispenser (Thermo Scientific) equipped with a small tube dispensing cassette (Thermo Scientific) unless otherwise stated. All KDM5 AlphaScreen assays were carried out in white 384-well proxiplates plus (PerkinElmer, code 6008280). Compounds for IC₅₀ determination were dissolved in 100% DMSO to a concentration of 10 mM and an 11-point, 3-fold dilution of each compound for IC₅₀ was dry dispensed (100 nL) into 384-well proxiplates using an ECHO-550 acoustic dispenser. The final assay concentration range was 0.0006–100 μM. Then 100 nL of DMSO was dispensed into each well of column 12 and 2,4-PDCA (100 mM) was dispensed into each well of column 24. KDM5B and KDM5C were diluted to 4 nM in assay buffer, and 5 μL of KDM5 enzyme dispensed into each well of a 384-well proxiplate. Plates were sealed with an aluminum foil, centrifuged at 1000 rpm for 5 s, and compound allowed to preincubate with enzyme for 15 min at room temperature before addition of peptide substrate. Substrate was prepared in assay buffer (200 μM L-AA, 20 μM FAS, 0.2 μM H3K4Me₃ peptide, 10 μM 2OG) and 5 μL dispensed into each well to initiate the enzyme reaction. Plates were sealed with an aluminum foil centrifuged at 1000 rpm for 15 s, and the enzyme reaction incubated at room temperature for 20 min. Enzyme reactions were stopped after 20 min by addition of 5 μL of assay buffer containing EDTA (30 mM) and NaCl (1.2 M). AlphaScreen detection reagent was prepared by diluting AlphaScreen streptavidin donor and protein A acceptor beads in assay buffer (0.08 mg/mL with respect to each bead) containing anti-H3K4Me₂ antibody (1:750) and preincubated for 1 h. Product H3K4Me₂ methyl mark was detected by addition of 5 μL of detection reagent followed by 2 h incubation at room temperature. After 2 h, plates were read in a BMG Labtech plate reader equipped with an AlphaScreen 680 nm/570 nm optic module. Data were normalized to the no enzyme (2,4-PDCA) control and IC₅₀ determined from nonlinear regression curve fitting using Graphpad Prism 5.0.

KDM2A, KDM3A, and KDM6B AlphaScreen Biochemical Assays. IC₅₀ values were determined as previously described.³⁴

Computational Chemistry. An enzyme–substrate cocrystal structure of KDM4A (PDB 3PDQ)³³ was prepared for modeling using Protein Preparation Wizard in Maestro,⁴⁷ and all water molecules not coordinating to the catalytic metal were removed. To propose predicted binding modes of the hit series, Glide (Grid-based Ligand Docking with Energetics)⁴⁸ was used for the docking experiments. The receptor grid was defined by a grid box of 30 × 30 × 30 Å³ with a default inner box (10 × 10 × 10 Å³) centered on the cocrystallized ligand in PDB 3PDQ.

Ligands were prepared using LigPrep,⁴⁹ applying the OPLS_2005 force-field with possible tautomeric and ionization states within pH range 5.0–9.0 generated using Epik metal binding state settings. Using Extra Precision (XP) settings, flexible docking of ligands was constrained to the coordinates of the core, defined as the terminal pyridine ring of the cocrystallized ligand in PDB 3PDQ, with an RMSD tolerance of 1.0 Å. The docked poses with the lowest RMSD and state penalties were selected as the preferred solutions.

Crystal Structure Determinations. For KDM4A bound to compounds 15, 16, 37, 40, 52d, 53a, 54a, 54j, and 58: A previously established N-terminally His-tagged KDM4A construct (residues 1–359)³⁷ was produced in *Escherichia coli* and purified by nickel affinity chromatography, followed by tag removal with TEV protease, reverse nickel affinity, and gel filtration. The protein was stored at –80 °C at 10 mg/mL concentration in a buffer containing 10 mM HEPES pH 7.5 and 200 mM NaCl. Purified KDM4A was crystallized in the apo form at 18 °C using the hanging-drop vapor-diffusion method. The crystallization drops were composed of 1.5 μL of protein (7 mg/mL) and 1.5 μL of reservoir solution containing 12–16% (w/v) PEG4000 and 0.1 M BTP pH 7.5, placed over 800 μL of reservoir solution. Plate-like crystals typically grew in a week and were then soaked by addition of 0.75 μL of compound at 10–200 mM in DMSO directly to the drops, followed by 4–48 h incubation at 18 °C. Crystals were briefly transferred to cryoprotectant solution containing 14% (w/v) PEG4000, 75 mM BTP pH 7.5, and 25% (v/v) glycerol prior to freezing in liquid nitrogen.

For KDM4A bound to compound 30b: The same KDM4A protein was produced, purified, and stored as described previously.³⁷ A complex of KDM4A with compound 30b was formed by mixing 30 mg/mL protein in 20 mM HEPES pH 7.5, 5% (v/v) glycerol, 500 mM NaCl, and 0.5 mM TCEP with 100 mM compound 30b in DMSO to a final concentration of 5 mM. Then, cocrystallization was performed in sitting drop plates at 4 °C by mixing 100 nL of protein–ligand complex with 50 nL of reservoir solution containing 0.1 M Bis-Tris pH 5.9, 0.15 M ammonium sulfate, 13% (w/v) PEG3350, placed over 20 μL of reservoir solution. Plate-like crystals typically grew in a week. Prior to data collection, crystals were briefly transferred to a cryoprotectant solution consisting of the precipitation buffer supplemented with 25% (v/v) ethylene glycol and were subsequently flash cooled in liquid nitrogen.

For structures of KDM4D bound to compounds 30a and 44a: DNA encoding for KDM4D (residues 1–342) was cloned into an in-house pET-based vector pNIC28-Bsa4⁵⁰ using ligation-independent cloning. The resulting construct expressed the desired proteins with an N-terminal His₆-tag and tobacco etch virus (TEV) protease cleavage site (extension MHHHHHHSSGVDLGTENLYFQ*SM). The protein was produced in *E. coli* and purified by nickel affinity chromatography, followed by tag removal with TEV protease, reverse nickel affinity, and gel filtration. The protein was stored at –80 °C at 11 mg/mL in a buffer containing 10 mM HEPES pH 7.5, 0.5 M NaCl, 5% glycerol, and 0.5 μM TCEP.

KDM4D was crystallized in sitting drop plates at 20 °C by mixing 100 nL of protein complex with 50 nL of reservoir solution containing 0.1 M Bis-Tris pH 5.9, 0.15 M ammonium sulfate, and 11% (w/v) PEG3350, placed over 20 μL of reservoir solution. The crystals were soaked with compound 30a or 44a by mixing 0.5 μL of 10 mM compound (in 9 parts ethylene glycol/1 part DMSO) with 1.5 μL of reservoir solution and adding it to the crystals. The crystals were then flash frozen in liquid nitrogen after incubating them for 3 h.

For KDM5B bound to compound 52d: A KDM5B construct encoding regions Phe26–Ile770 was amplified from an Origene cDNA clone and cloned into a pFastBac-derived vector (pFB-LIC-Bse) containing a tobacco etch virus (TEV) protease cleavable N-terminal His₆-tag. The recombinant KDM5B (residues 26–770) construct was expressed in Sf9 cells, with generation of recombinant baculo viruses, insect cell culture, and infections being performed according to the manufacturer's instructions (Invitrogen). The cells were harvested 72 h post infection, lysed in a buffer containing 50 mM HEPES pH 7.5, 500 mM NaCl, 10 mM imidazole, 5% glycerol, 0.5 mM TCEP, and a protease inhibitor cocktail (Calbiochem) and purified using nickel affinity chromatography using a stepwise gradient of imidazole. The

eluted protein was then incubated with TEV protease at 4 °C overnight followed by size-exclusion chromatography (Superdex 200). The TEV protease and uncleaved protein were removed using nickel affinity chromatography, and protein was concentrated to 8.1 mg/mL and stored at -80 °C. Protein was crystallized at 4 °C using the sitting drop vapor diffusion method. KDM5B was preincubated with 4 mM MnCl₂ before the protein was transferred to crystallization plates. Crystals were obtained in drops consisting of 100 nL of protein mix (8.1 mg/mL), 200 nL of a precipitant consisting of 1.6 M Na/K phosphate, 0.1 M HEPES pH 7.5, and 20 nL of KDM5B seeds of crystals obtained from the same condition. Compound was soaked into apo crystals of KDM5B for 5 min at a concentration of 5 mM. Crystals were cryoprotected with mother liquor supplemented with 25% ethylene glycol before they were flash-frozen in liquid nitrogen.

Data Collection, Processing, and Refinement. X-ray data were collected in-house at the Institute of Cancer Research, London, UK, on a Rigaku FRX-AFC11-VariMax Cu-VHF-Pilatus300 K, at the Structural Genomics Consortium, Oxford, UK, on a Bruker Microstar generator equipped with an APEX II detector, at Diamond Light Source, Oxfordshire, UK, at beamlines I02, I03, I04, and I04-I, and at the European Synchrotron Ray Facility, Grenoble, France, at beamline ID23. Crystals of KDM4A belonged to the space group *P*1₂,1 (or *P*2₁,2 for KDM4A bound to compound **30b**) and diffracted to resolutions between 2.05 and 2.65 Å. Crystals of KDM4D belonged to the space group *P*4₃,2,2 and diffracted to resolutions between 1.41 and 1.88 Å. The KDM5B crystal belonged to the space group *P*6₃,22 and diffracted to a resolution of 2.35 Å. All data sets were integrated with XDS,⁵¹ scaled, and merged with AIMLESS,⁵² except for data sets collected on the Bruker system which were integrated with SAINT (version 8.3, Bruker AXS Inc., 2013) and scaled with SADABS (version 2012/1, Bruker AXS Inc., 2012). The structures were solved by molecular replacement using PHASER,^{53,54} and publicly available KDM4A, KDM4D, and KDM5B structures (PDB codes 2OQ7, 3DXT, and 5A1F, respectively)³⁷ with ligand and water molecules removed were used as molecular replacement models. The protein–ligand structures were manually corrected and rebuilt in COOT⁵⁵ and refined with BUSTER,⁵⁶ Phenix,⁵⁷ or REFMAC⁵⁸ in iterative cycles. Ligand restraints were generated with GRADE⁵⁹ and MOGUL.⁶⁰ The quality of the structures was assessed with MOLPROBITY.^{61,62} The data collection and refinement statistics are presented in Supporting Information, Table S1.

Caco-2 Permeability. *P*_{app} (apparent permeability) was determined in the Caco-2 human colon carcinoma cell line. Cells were maintained (DMEM with 10% fetal bovine serum, penicillin, and streptomycin) in a humidified atmosphere with 5%CO₂/95% air for 10 days. Cells were plated out onto a cell culture assembly plate (Millipore, UK), and monolayer confluency was checked using a TEER electrode prior to the assay. Media was washed off and replaced in the appropriate apical and basal wells with HBSS buffer (pH7.4) containing compound (10 μM, 1% DMSO). The Caco-2 plate was incubated for 2 h at 37 °C, and Lucifer Yellow was used to confirm membrane integrity after the assay. Samples from the apical and basolateral chambers were analyzed using Waters TQ-S LC-MS/MS.

Cell-Based Assays.⁴⁵ Full length cDNA for KDM4A (JMJD2A, O75164) and KDM5B (JARID1B, Q9UGL1) were amplified by PCR and cloned into the pDONR-221 vector using a Gateway BP reaction. To produce catalytically inactive KDMs, residues involved in iron coordination were mutated to alanine (KDM5B, H499A/E501A; KDM4A, H188A/E190A). Mutations were introduced into the full length KDM Gateway entry clones using 15 cycles of the QuikChange II PCR protocol (Agilent Technologies). Mammalian expression constructs encoding N-terminal 3×FLAG were constructed by a Gateway LR recombination reaction between pCDNAS-FRT/TO-3FLAG destination vector (PMID: 24412199) and the wild-type or mutated KDM Gateway entry clone.

The human cervical carcinoma cell line HeLa was obtained from the American Type Cultures Collection and maintained in Eagle's Minimal Essential Media (Sigma-Aldrich) supplemented with 10% heat-inactivated FBS (Life Technologies). Cells were transiently transfected with either the Flag-tagged demethylase or an inactive version containing mutations in the catalytic site using Lipofectamine 3000

(Life Technologies). Four hours after transfection, the cells were treated with serial dilutions of compound **54k** for 24 h. The cells were then fixed and stained with a mouse monoclonal anti-Flag (Sigma F3165) and with either a rabbit anti-H3K9me3 1 h at RT (Abcam ab8898) or a rabbit anti-H3K4me3 overnight at 4 °C (Diagenode C15410003). The secondary antibodies were goat antirabbit Alexa Fluor 488 (Life Technologies A11034) and goat antimouse Alexa Fluor 568 (Life Technologies A21124). Image acquisition was conducted using the Operetta high content imaging system (PerkinElmer), and image analysis was performed with the Columbus software (PerkinElmer). After the DAPI-stained nuclei were automatically identified, a minimum threshold for anti-Flag intensity was set so that only cells highly expressing the demethylase were analyzed.

Microsomal and Aldehyde Oxidase (AO) Clearance Studies. CYP450 and AO-mediated metabolism of KDM4 inhibitor compounds were assessed by incubation of compound (1 μM concentration) in mouse and human liver microsomes (MLM, HLM) and mouse liver cytosol (0.5 mg/mL) (Tebu-bio) respectively in 0.1 M PBS at 37 °C.⁶³ Microsomal incubations were initiated by addition of NADPH and UDPGA for phase I and II reactions. Cytosol incubations were initiated by KDM4 inhibitor compounds in the presence and absence of AO inhibitor raloxifene. Compound levels were measured over time (0, 5, 10, 15, and 30 min) to calculate clearance by removing aliquots of the incubate at specific time points and quenching into acetonitrile with internal standard (IS) and centrifugation at 3000 rpm for 30 min at 4 °C. Supernatant was diluted for LC-MS/MS analysis.

Chemistry. Commercially available starting materials, reagents, and anhydrous solvents were used as supplied. Flash column chromatography was performed using Merck silica gel 60 (0.025–0.04 mm). Thin layer chromatography was performed using Merck Millipore TLC silica gel 60 F₂₅₄ aluminum sheets and visualized by UV (254 and 280 nm), iodine, and KMnO₄. Column chromatography was also performed on a FlashMaster personal unit using isolute Flash silica columns or a Biotage Isolera purification system using Biotage KP-SNAP cartridges. Ion exchange chromatography was performed using acidic Isolute Flash SCX-II cartridges or basic Isolute Flash NH₂ cartridges. ¹H NMR spectra were recorded on either a Bruker Avance-500 or Bruker Avance-400 NMR machine. Samples were prepared as solutions in a deuterated solvent and referenced to the appropriate internal nondeuterated solvent peak or tetramethylsilane. Chemical shifts were recorded in ppm (δ) downfield of tetramethylsilane.

LC-MS Analysis. Analysis was performed on a Waters LCT with a Waters Alliance 2795 separations module and Waters 2487 dual wavelength absorbance detector coupled to a Waters/Micromass LCT time-of-flight mass spectrometer with ESI source.

Method A: Analytical separation was carried out at 30 °C on a Merck Purospher STAR column (RP-18e, 30 mm × 4 mm) using a flow rate of 1.5 mL/min in a 4 min gradient elution with detection at 254 nm. The mobile phase was a mixture of methanol (solvent A) and water (solvent B), both containing formic acid at 0.1%. Gradient elution was as follows: 10:90 (A/B) to 90:10 (A/B) over 2.5 min, 90:10 (A/B) for 1 min, and then reversion back to 10:90 (A/B) over 0.3 min, finally 10:90 (A/B) for 0.2 min.

Analysis was also performed on an Agilent 1200 series HPLC and diode array detector coupled to a 6210 time-of-flight mass spectrometer with dual multimode APCI/ESI source.

Method B: Analytical separation was carried out at 30 °C on a Merck Purospher STAR column (RP-18e, 30 mm × 4 mm) using a flow rate of 1.5 mL/min in a 4 min gradient elution with detection at 254 nm. The mobile phase was a mixture of methanol (solvent A) and water (solvent B), both containing formic acid at 0.1%. Gradient elution was as follows: 10:90 (A/B) to 90:10 (A/B) over 2.5 min, 90:10 (A/B) for 1 min, and then reversion back to 10:90 (A/B) over 0.3 min, finally 10:90 (A/B) for 0.2 min.

Method C: Analytical separation was carried out at 40 °C on a Merck Purospher STAR column (RP-18e, 30 mm × 4 mm) using a flow rate of 3 mL/min in a 2 min gradient elution with detection at 254 nm. The mobile phase was a mixture of methanol (solvent A) and water (solvent B), both containing formic acid at 0.1%. Gradient elution was as follows: 10:90 (A/B) to 90:10 (A/B) over 1.25 min, 90:10 (A/B) for 0.5 min,

and then reversion back to 10:90 (A/B) over 0.15 min, finally 10:90 (A/B) for 0.1 min.

Method D: Analytical separation was carried out at 40 °C on a Merck Chromolith Flash column (RP-18e, 25 mm × 2 mm) using a flow rate of 1.5 mL/min in a 2 min gradient elution with detection at 254 nm. The mobile phase was a mixture of methanol (solvent A) and water (solvent B), both containing formic acid at 0.1%. Gradient elution was as follows: 5:95 (A/B) to 100:0 (A/B) over 1.25 min, 100:0 (A/B) for 0.5 min, and then reversion back to 5:95 (A/B) over 0.05 min, finally 5:95 (A/B) for 0.2 min.

Method E: Analytical separation was carried out at 30 °C on a Merck Chromolith Flash column (RP-18e, 25 mm × 2 mm) using a flow rate of 0.75 mL/min in a 4 min gradient elution with detection at 254 nm. The mobile phase was a mixture of methanol (solvent A) and water (solvent B), both containing formic acid at 0.1%. Gradient elution was as follows: 5:95 (A/B) to 100:0 (A/B) over 2.5 min, 100:0 (A/B) for 1 min, and then reversion back to 5:95 (A/B) over 0.1 min, finally 5:95 (A/B) for 0.4 min.

Analysis was also performed on a Waters Acquity UPLC and diode array detector coupled to a Waters G2 QToF mass spectrometer fitted with a multimode ESI/APCI source.

Method F: Analytical separation was carried out at 30 °C on a Phenomenex Kinetex XB-C18 column (30 mm × 2.1 mm, 1.7 μ, 100 Å) using a flow rate of 0.5 mL/min in a 2 min gradient elution with detection at 254 nm. The mobile phase was a mixture of methanol (solvent A) and water (solvent B), both containing formic acid at 0.1%. Gradient elution was as follows: 10:90 (A/B) to 90:10 (A/B) over 1.25 min, 90:10 (A/B) for 0.5 min, and then reversion back to 10:90 (A/B) over 0.15 min, finally 10:90 (A/B) for 0.1 min.

Method G: Analytical separation was carried out at 30 °C on a Phenomenex Kinetex XB-C18 column (30 mm × 2.1 mm, 1.7 μ, 100 Å) using a flow rate of 0.3 mL/min in a 4 min gradient elution with detection at 254 nm. The mobile phase was a mixture of methanol (solvent A) and water (solvent B), both containing formic acid at 0.1%. Gradient elution was as follows: 10:90 (A/B) to 90:10 (A/B) over 3 min, 90:10 (A/B) for 0.5 min, and then reversion back to 10:90 (A/B) over 0.3 min, finally 10:90 (A/B) for 0.2 min.

Method H: Analytical separation was carried out at 30 °C on a Phenomenex Kinetex C18 column (30 mm × 2.1 mm, 2.6 μ, 100 Å) using a flow rate of 0.5 mL/min in a 2 min gradient elution with detection at 254 nm. The mobile phase was a mixture of methanol (solvent A) and water (solvent B), both containing formic acid at 0.1%. Gradient elution was as follows: 10:90 (A/B) to 90:10 (A/B) over 1.25 min, 90:10 (A/B) for 0.5 min, and then reversion back to 10:90 (A/B) over 0.15 min, finally 10:90 (A/B) for 0.1 min.

Method I: Analytical separation was carried out at 30 °C on a Phenomenex Kinetex C18 column (30 mm × 2.1 mm, 2.6 μ, 100 Å) using a flow rate of 0.3 mL/min in a 4 min gradient elution with detection at 254 nm. The mobile phase was a mixture of methanol (solvent A) and water (solvent B), both containing formic acid at 0.1%. Gradient elution was as follows: 10:90 (A/B) to 90:10 (A/B) over 3 min, 90:10 (A/B) for 0.5 min, and then reversion back to 10:90 (A/B) over 0.3 min, finally 10:90 (A/B) for 0.2 min.

Analysis was also performed on a Waters system equipped with a Waters 2545 binary gradient module, a Waters SQ-Detector 2, Waters 2489 UV/visible detector, and a Waters 2424 ELS detector.

Method J: Analytical separation was carried out on a Kinetex 5u EVO C18 column (100 mm × 3.0 mm, 100 Å) using a flow rate of 2 mL/min in a 3 min gradient elution. The mobile phase was a mixture of 93% H₂O, 5% acetonitrile, and 2% of 0.5 M ammonium acetate adjusted to pH 6 with glacial acetic acid (solvent A) and 18% H₂O, 80% acetonitrile, and 2% of 0.5 M ammonium acetate adjusted to pH 6 with glacial acetic acid (solvent B). Gradient elution was as follows: 95:5 (A/B) 0.35 min, 95:5 (A/B) to 5:95 (A/B) over 1 min, 5:95 (A/B) over 0.75 min, and then reversion back to 95:5 (A/B) over 0.1 min and 95:5 (A/B) over 0.8 min.

Method K: Analytical separation was carried out on a Chromolith Performance RP-18e column (100 mm × 2.0 mm) using a flow rate of 1.5 mL/min in a 5 min gradient elution. The mobile phase was a mixture of 93% H₂O, 5% acetonitrile, and 2% of 0.5 M ammonium acetate adjusted to pH 6 with glacial acetic acid (solvent A) and 18% H₂O, 80% acetonitrile and 2% of 0.5 M ammonium acetate adjusted to pH 6 with

glacial acetic acid (solvent B). Gradient elution was as follows: 95:5 (A/B) over 0.5 min, 95:5 (A/B) to 5:95 (A/B) over 2 min, 5:95 (A/B) over 1 min, then reversion back to 95:5 (A/B) over 0.1 min and 95:5 (A/B) over 1.4 min.

Method L: Analytical separation was carried out on a Waters sunfire C18 column (4.6 mm × 150 × 4.6 mm, 100 Å) using a flow rate of 1 mL/min in a 20 min gradient run. The mobile phase was a mixture of 99.99% water and 0.01% CF₃CO₂H (solvent A) and 99.99% acetonitrile and 0.01% CF₃CO₂H (solvent B). Gradient elution was as follows: 100:0 (A/B) over 2 min, 100:0 (A/B) to 0:100 (A/B) over 16 min and 0:100 (A/B) over 2 min. All compounds submitted for biological testing were determined to be >95% pure by Methods A–L unless stated otherwise.

LC-HRMS Analysis. LC-HRMS was performed using either an Agilent 1200 series HPLC and diode array detector coupled to a 6210 time-of-flight mass spectrometer with dual multimode APCI/ESI source (methods B and E) or a Waters Acquity UPLC and diode array detector coupled to a Waters G2 QToF mass spectrometer fitted with a multimode ESI/APCI source (methods G and I) or on an Agilent 1290 uHPLC system coupled with an Agilent ESI-QTOF 6530 mass spectrometer (method J). LC-HRMS methods B and E referenced to caffeine [M + H]⁺ 195.087652, reserpine [M + H]⁺ 609.280657 (method B), or hexakis (2,2-difluoroethoxy)phosphazene [M + H]⁺ 622.02896 (methods B and E) and hexakis(1H,1H,3H-tetrafluoropentoxy)phosphazene [M + H]⁺ 922.009798. LC-HRMS methods G and I referenced to leucine enkephalin fragment ion [M + H]⁺ 397.1876. LC-HRMS method J referenced to hexakis (2,2-difluoroethoxy)phosphazene [M + H]⁺ 622.02896 and hexakis(1H,1H,3H-tetrafluoropentoxy)phosphazene [M + H]⁺ 922.009798.

General Procedure 1: Amine Displacement of Mesylate Using Cesium Carbonate. Cesium carbonate (3 equiv) was added to a mesylate intermediate freshly made from alcohol 47 (1 equiv) and amine (2 equiv) in anhydrous DMF under N₂. The reaction mixture was stirred for 15 h at 90 °C and monitored by LCMS. The reaction mixture was diluted in water and extracted three times with EtOAc. The combined organic layers were washed with saturated brine solution, dried over MgSO₄, and concentrated in vacuo to give the crude material which was purified by Biotage column chromatography (see individual compounds for details of the eluent used).

General Procedure 2: Amine Displacement of Mesylate Using Trimethylamine. Triethylamine (2 equiv) was added to a solution of mesylate intermediate freshly made from alcohol 47 (1 equiv) and amine [or amine hydrochloride] (1.2 equiv) in anhydrous DMF under N₂. The reaction mixture was heated at 50 °C for 15 h and monitored by LCMS. When the reaction had gone to completion, the reaction mixture was diluted in H₂O and extracted three times with EtOAc. The combined organic layers were washed with saturated LiCl solution and saturated brine solution, dried over MgSO₄, and concentrated in vacuo to give the crude material which was purified by Biotage column chromatography (see individual compounds for details of the eluent used).

General Procedure 3: Reductive Amination. To a microwave vial was added the required aldehyde (1 equiv) and corresponding amine (1.5 equiv) and the flask purged with argon. Anhydrous 1,2-dichloroethane (4 mL) was then added, the mixture was stirred to allow dissolution followed by the addition of sodium triacetoxyborohydride (1.6 equiv), the vial was capped, and the mixture was stirred at room temperature overnight. Once the reaction was deemed complete by LCMS analysis, the mixture was directly absorbed onto silica gel and purified by flash column chromatography to afford the requisite amine (workup procedure A). Alternatively, the mixture was concentrated to afford an amorphous solid and passed through a plug of silica eluting with 40% MeOH/CH₂Cl₂ to afford an oil which was used without further purification (workup procedure B).

General Procedure 4: SEM Deprotection with 6 M HCl/THF. Hydrochloric acid (6 M, 60–90 equiv) was added to a solution of SEM protected material (1 equiv) in THF (0.1 M). The reaction mixture was stirred at 50–60 °C for between 3 and 8 h and monitored by LCMS. Following completion of the reaction, the reaction mixture was concentrated in vacuo and purified by Biotage column chromatography on a KP-NH snap column unless otherwise stated (see individual compounds for details of the eluent used). The product obtained from

column chromatography was triturated with Et₂O to give the pure product.

General Procedure 5: SEM Deprotection with HCl/1,4-Dioxane. To a microwave vial was added the SEM protected starting material (1 equiv), 1,4-dioxane (3 mL), and distilled water (1 mL) followed by the dropwise addition of HCl in dioxane (4M, 25 equiv). The vial was capped and the mixture stirred at 50 °C until analysis by LCMS indicated complete conversion to the product. The mixture was then concentrated and passed through an SCX-2 cartridge washing initially with MeOH and then NH₃/MeOH. The basic wash was concentrated and triturated with Et₂O to afford a solid. If necessary, the solid was further purified by flash column chromatography on a SNAP KP-NH column eluting with 0–40% EtOH/CH₂Cl₂.

3-(Ethylsulfonyl)-N-(4-(pyridin-2-yl)thiazol-2-yl)benzamide (7c). To a mixture of 3-(ethylsulfonyl)benzoic acid (0.098 g, 0.46 mmol, 1 equiv), 1-hydroxybenzotriazole hydrate (0.068 g, 0.50 mmol, 1.1 equiv), EDCI (0.105 g, 0.55 mmol, 1.2 equiv), and anhydrous CH₂Cl₂ (4 mL, 0.12 M) was added 2-amino-4-(2-pyridyl)thiazole (0.085 g, 0.48 mmol, 1.05 equiv). The reaction mixture was stirred at room temperature for 4 h under argon, then diluted with CH₂Cl₂ (50 mL) and washed with a saturated NaHCO₃ solution (2 × 20 mL) and saturated brine solution (20 mL), dried (Na₂SO₄), and concentrated in vacuo. This residue was absorbed on silica gel and the free running powder was placed on a 20 g Isolute silica II column which was eluted with 30% EtOAc in CH₂Cl₂, 70% EtOAc in CH₂Cl₂, and finally 2% MeOH in EtOAc/CH₂Cl₂ (v/v; 4:1). The title compound was obtained as a white solid (0.068 g, 40%). ¹H NMR (500 MHz, DMSO-*d*₆) δ 1.15 (t, *J* = 7.2 Hz, 3H), 3.42 (q, *J* = 7.2 Hz, 2H), 7.36 (ddd, *J* = 1.2, 4.8, 7.5 Hz, 1H), 7.87 (t, *J* = 7.9 Hz, 1H), 7.91 (td, *J* = 1.9, 7.8 Hz, 1H), 7.94 (s, 1H), 8.02 (d, *J* = 7.8 Hz, 1H), 8.15 (dt, *J* = 1.3, 7.8 Hz, 1H), 8.44 (dt, *J* = 1.3, 7.8 Hz, 1H), 8.61–8.64 (m, 2H), 13.15 (s, 1H). LC-MS (method B, ESI, *m/z*) *t*_R = 2.50 min –374 (M + H)⁺. HRMS (method B): found, 374.0610; calculated for C₁₇H₁₆N₃O₃S₂ (M + H)⁺, 374.0628.

Methyl 2-(1-Ethoxyvinyl)isonicotinate (12). To a mixture of methyl 2-bromoisonicotinate (0.80 g, 3.7 mmol, 1 equiv), tributyl(1-ethoxyvinyl)stannane (1.44 g, 4.0 mmol, 1.1 equiv), and 1,4-dioxane (20 mL, 0.19 M) was added tetrakis(triphenylphosphine)palladium (0.300 g, 0.173 mmol, 5 mol %). The reaction mixture was heated at reflux (120 °C) for 18 h under nitrogen, cooled to room temperature, and then concentrated in vacuo. The residue was purified by silica gel column chromatography eluting with CH₂Cl₂:hexane (2:1) to afford the desired product as a yellow oil which solidified on standing (0.500 g, 65%). ¹H NMR (500 MHz, CDCl₃) δ 1.34 (t, *J* = 7.0 Hz, 3H), 3.95 (s, 3H), 3.98 (q, *J* = 7.0 Hz, 2H), 4.41 (d, *J* = 2.1 Hz, 1H), 5.45 (d, *J* = 2.1 Hz, 1H), 7.73 (dd, *J* = 1.6, 5.0 Hz, 1H), 8.19 (t, *J* = 1.0 Hz, 1H), 8.69 (dd, *J* = 0.8, 5.0 Hz, 1H). LC-MS (method C; ESI, *m/z*) *t*_R = 1.4 min –208 (M + H)⁺.

Methyl 2-(2-Bromoacetyl)isonicotinate (13). A mixture of methyl 2-(1-ethoxyvinyl)isonicotinate (0.500 g, 2.41 mmol) and 1-bromopyrrolidine-2,5-dione (0.429 g, 2.41 mmol) was suspended in 10% water in THF:H₂O (2:0.2 mL). The reaction was stirred at room temperature for 1 h. Volatiles were removed in vacuo and the residue purified by flash silica gel column chromatography eluting with 30% hexane in dichloromethane. The pure fractions provided the desired product as a pale-brown oil which solidified on standing (0.38 g, 61%). ¹H NMR (500 MHz, CDCl₃) δ 4.00 (s, 3H), 4.84 (s, 2H), 8.07 (dd, *J* = 1.7, 5.0 Hz, 1H), 8.59 (dd, *J* = 0.9, 1.7 Hz, 1H), 8.84 (dd, *J* = 0.7, 5.0 Hz, 1H). LC-MS (method C; ESI, *m/z*) *t*_R = 1.25 min –258, 260 [(M + H)⁺, Br isotopic pattern]. For the synthesis of compound 25, this intermediate was prepared from methyl 2-acetylpyridine-4-carboxylate as follows: To a “paste like” mixture of methyl 2-acetylpyridine-4-carboxylate (1.79 g, 10.0 mmol), acetic acid (12.5 mL), and 48% aqueous HBr (1.12 mL, 10.0 mmol) cooled in an ice-bath, bromine (0.57 mL, 11.0 mmol) was added dropwise. The ice-bath was removed, and stirring was continued at room temperature for 1 h under argon, then at 75 °C for 1.5 h under argon. The reaction mixture was cooled to room temperature with the aid of an ice-bath, diluted with THF (12 mL), and stirred at room temperature for 20 min and allowed to stand overnight at room temperature; the volatiles were then removed under vacuo. The residue was diluted with EtOAc (130 mL), and to this

solution a saturated NaHCO₃ solution (50 mL) was carefully added. The two layers were separated, and the organic layer was carefully washed with more saturated NaHCO₃ solution (30 mL) and water (20 mL), dried (Na₂SO₄), and concentrated in vacuo. The liquid residue was absorbed onto silica gel and placed on a 50 g Isolute silica II column which was eluted with 5%, 10%, and finally 15% EtOAc in hexane to provide in order of elution the dibrominated product, and the title compound as an oily residue which solidified on standing at room temperature (0.98 g, 38%). ¹H NMR and LC-MS as reported above.

Methyl 2-(2-((tert-Butoxycarbonyl)amino)thiazol-4-yl)isonicotinate (14). A mixture of methyl 2-(2-bromoacetyl)isonicotinate (0.100 g, 0.387 mmol, 1 equiv), *N*-Boc-thiourea (0.068 g, 0.387 mmol, 1 equiv), and triethylamine (0.04 g, 0.4 mmol, 1.05 equiv) was suspended in ethanol (10 mL, 0.04 M) and heated under reflux for 1 h. The reaction was concentrated in vacuo and the residue purified by flash silica gel column chromatography eluting with 5% EtOAc in CH₂Cl₂ to give the product as a yellow oil which solidified on standing (0.072 g, 56%). ¹H NMR (500 MHz, CDCl₃) δ 1.50 (s, 9H), 3.98 (s, 3H), 7.76 (s, 1H), 7.78 (dd, *J* = 1.6, 5.0 Hz, 1H), 8.47 (s, 1H), 8.62 (br s, 1H), 8.76 (d, *J* = 4.9 Hz, 1H). LC-MS (method C; ESI, *m/z*) *t*_R = 1.56 min –336 (M + H)⁺.

2-(2-Aminothiazol-4-yl)isonicotinic Acid (15). A solution of 4 M HCl in dioxane (1 mL) was added to methyl 2-(2-((tert-butoxycarbonyl)amino)thiazol-4-yl)isonicotinate (0.022 g, 0.066 mmol). The mixture was stirred at room temperature for 1 h. Volatiles were removed in vacuo, and the residue was passed through an isolute-NH₂ cartridge eluting with methanol to afford a brown solid which was dissolved in THF (2 mL) and NaOH solution (3.3 M, 0.3 mL). After stirring at room temperature for 1 h, acetic acid (0.06 g, 1.0 mmol) was added and the solution was evaporated to dryness. Water (1 mL) was added to the residue and a white powder separated out which was filtered and dried (8 mg, 55%). ¹H NMR (500 MHz, DMSO-*d*₆) δ 7.18 (s, 2H), 7.31 (s, 1H), 7.66 (dd, *J* = 1.6, 5.0 Hz, 1H), 8.30 (s, 1H), 8.68 (d, *J* = 5.0 Hz, 1H), 14.00 (br s, 1H). LC-MS (method C); ESI, *m/z*) *t*_R = 0.56 min –222 (M + H)⁺. HRMS (method B): found, 222.0333; calculated for C₉H₈N₃O₂S (M + H)⁺, 222.0332.

3-Amino-2-chloroisonicotinic Acid (32). To a solution of methyl 3-amino-2-chloroisonicotinate (1.00 g, 5.36 mmol, 1 equiv) in methanol (13 mL, 0.4 M) was added 1 M aqueous sodium hydroxide (14.4 mL, 14.4 mmol), and the reaction was stirred at room temperature for 45 min. Methanol was removed in vacuo, and the remaining aqueous solution was acidified to pH 5.5 by addition of 1 M HCl. A white precipitate formed which was filtered and dried (0.715 g, 77%). ¹H NMR (500 MHz, DMSO-*d*₆) δ 6.80 (br s, 2H), 7.58 (d, *J* = 5.0 Hz, 1H), 7.61 (d, *J* = 5.0 Hz, 1H), 13.80 (br s, 1H). LC-MS (method C; ESI, *m/z*) *t*_R = 0.83 min –173, 175 [(M + H)⁺ Cl isotopic pattern].

3-Amino-2-chloroisonicotinamide (33). To a stirred solution of 3-amino-2-chloroisonicotinic acid (0.750 g, 4.35 mmol) in thionyl chloride (10 mL) was added 2 drops of DMF and the reaction heated at reflux under nitrogen for 2 h. Volatiles were removed and the residue was suspended in anhydrous THF (10 mL) and was slowly added to a solution of ammonium hydroxide (10 mL) cooled in an ice bath and the reaction stirred at room temperature for 1.5 h. EtOAc (40 mL) and CH₂Cl₂ (10 mL) were added and the layers separated. The organic solution was dried and concentrated in vacuo. The residue obtained was purified by flash silica gel column chromatography eluting with 20% hexane in ethyl acetate to afford the desired product as a white powder (0.664 g, 89%). ¹H NMR (500 MHz, DMSO-*d*₆) δ 6.76 (br s, 2H), 7.50 (d, *J* = 5.1 Hz, 1H), 7.61 (d, *J* = 5.1 Hz, 1H), 7.67 (br s, 1H), 8.18 (br s, 1H). LC-MS (method A; ESI, *m/z*) *t*_R = 0.52 min –172, 174 [(M + H)⁺ Cl isotopic pattern].

8-Chloropyrido[3,4-*d*]pyrimidin-4(3H)-one (34).⁴⁰ 3-Amino-2-chloroisonicotinamide (0.60 g, 3.5 mmol) in anhydrous triethoxyethane (15 mL) was heated at reflux (160 °C) for 18 h. The reaction was cooled to room temperature, and the pale-white powder was filtered and washed with Et₂O (2 × 5 mL) then dried to give the product as a white solid (0.52 g, 82%). ¹H NMR (500 MHz, DMSO-*d*₆) δ 7.96 (d, *J* = 5.1 Hz, 1H), 8.32 (s, 1H), 8.42 (d, *J* = 5.1 Hz, 1H), 12.85 (br s, 1H). LC-MS (method H; ESI, *m/z*) *t*_R = 0.66 min –182, 184 [(M + H)⁺ Cl

isotopic pattern]. HRMS (method I): found, 182.0125; calculated for $C_7H_4N_3ClO$ ($M + H$)⁺, 182.0121.

8-Chloro-3-((2-(trimethylsilyl)ethoxy)methyl)pyrido[3,4-*d*]pyrimidin-4(3*H*)-one (35). 8-Chloropyrido[3,4-*d*]pyrimidin-4(3*H*)-one (1.87 g, 10.3 mmol, 1 equiv) was dissolved in dry DMF (15 mL, 0.7 M). The solution was heated to 60 °C, and potassium carbonate (2.85 g, 20.6 mmol, 2 equiv) was added. After 5 min of stirring, (2-(chloromethoxy)ethyl)trimethylsilane (2.06 g, 12.36 mmol, 1.2 equiv) was slowly added. Stirring was continued at 60 °C for 4 h, the reaction cooled to room temperature, and EtOAc (60 mL) was added. The heterogeneous mixture was washed with water (2 × 60 mL), dried (Na_2SO_4), and concentrated in vacuo. The crude product was purified by silica gel column chromatography eluting with 3% EtOAc in CH_2Cl_2 to provide the title compound as a white powder (2.7 g, 84%). ¹H NMR (500 MHz, $CDCl_3$) δ 0.01 (s, 9H), 0.97–1.00 (m, 2H), 3.67–3.71 (m, 2H), 5.46 (s, 2H), 8.06 (d, *J* = 5.1 Hz, 1H), 8.34 (s, 1H), 8.49 (d, *J* = 5.1 Hz, 1H). LC-MS (method H; ESI, *m/z*) *t*_R = 1.4 min (100% purity) –254, 256 [(*M* – SEM + TMS)⁺, Cl isotopic pattern]. This compound was also prepared in lower yield (55 to 65%) by performing the reaction at room temperature.

4-(2-((*tert*-Butyldimethylsilyl)oxy)ethyl)-1*H*-pyrazole (45). *tert*-Butylchlorodimethylsilane (7.09 g, 47.0 mmol, 1.05 equiv) was added to a solution of 1*H*-imidazole (3.35 g, 49.2 mmol, 1.1 equiv) and 2-(1*H*-pyrazol-4-yl)ethanol (5.02 g, 44.8 mmol, 1 equiv) in DMF (50 mL, 0.9 M) at room temperature. The resultant solution was stirred for 30 min at room temperature and monitored by LCMS. On completion, the reaction mixture was diluted with water (100 mL) and extracted three times with EtOAc (3 × 100 mL). The combined organic layers were washed with saturated lithium chloride solution (150 mL) and saturated brine solution (150 mL) and dried over $MgSO_4$. The filtrate was concentrated in vacuo to give the product as a clear, pale-yellow oil (9.63 g, 95%). ¹H NMR (500 MHz, $CDCl_3$) δ 0.04 (s, 6H), 0.91 (s, 9H), 2.73 (t, *J* = 6.8 Hz, 2H), 3.76 (t, *J* = 6.8 Hz, 2H), 7.47 (s, 2H), NH signal not observed. LC-MS (method C; ESI, *m/z*) *t*_R = 1.46 min –227 [(*M* + H)⁺]. HRMS (method B): found, 227.1580; calculated for $C_{11}H_{23}N_2OSi$ ($M + H$)⁺, 227.1574.

8-(4-(2-((*tert*-Butyldimethylsilyl)oxy)ethyl)-1*H*-pyrazol-1-yl)-3-((2-(trimethylsilyl)ethoxy)methyl)pyrido[3,4-*d*]pyrimidin-4(3*H*)-one (46). Note: when attempted at scale, these reactions were carried out in batches, generally using ~150 mg portions of 8-chloro-3-((2-(trimethylsilyl)ethoxy)methyl)pyrido[3,4-*d*]pyrimidin-4(3*H*)-one per microwave vial. Cesium carbonate (1.33 g, 4.09 mmol, 2 equiv) and 4-(2-((*tert*-butyldimethylsilyl)oxy)ethyl)-1*H*-pyrazole (920 mg, 4.06 mmol, 2 equiv) were added to a microwave vial equipped with a stirrer bar. This was sealed and evacuated and flushed with N_2 . Anhydrous MeCN (14 mL, 0.15 M) was added to the vial and the reaction mixture stirred for 20 min under N_2 at room temperature. The cap was then removed, 8-chloro-3-((2-(trimethylsilyl)ethoxy)methyl)pyrido[3,4-*d*]pyrimidin-4(3*H*)-one (637 mg, 2.04 mmol, 1 equiv) was added, the vial resealed, and evacuated and flushed with N_2 . The reaction mixture was then stirred at reflux for 18 h. Solids were removed by filtration and rinsed with CH_2Cl_2 (3 × 15 mL). The filtrate was concentrated in vacuo and purified by Biotage column chromatography on a KP-Sil snap cartridge (30% EtOAc in cyclohexane) to give the title product as a pale-yellow solid (724 mg, 71%). ¹H NMR (500 MHz, $CDCl_3$) δ 0.01 (s, 9H), 0.06 (s, 6H), 0.91 (s, 9H), 0.95–1.00 (m, 2H), 2.80 (t, *J* = 6.7 Hz, 2H), 3.67–3.71 (m, 2H), 3.84 (t, *J* = 6.7 Hz, 2H), 5.47 (s, 2H), 7.79 (s, 1H), 8.05 (d, *J* = 5.1 Hz, 1H), 8.29 (s, 1H), 8.61 (s, 1H), 8.63 (d, *J* = 5.1 Hz, 1H). LC-MS (method C; ESI, *m/z*) *t*_R = 1.79 min –502 [(*M* + H)⁺]. HRMS (method B): found, 502.2672; calculated for $C_{24}H_{40}N_5O_3Si_2$ ($M + H$)⁺, 502.2670.

8-(4-(2-Hydroxyethyl)-1*H*-pyrazol-1-yl)-3-((2-(trimethylsilyl)ethoxy)methyl)pyrido[3,4-*d*]pyrimidin-4(3*H*)-one (47). Hydrochloric acid (1 M, 5.5 mL, 10 equiv) was added to a solution of 8-(4-(2-((*tert*-butyldimethylsilyl)oxy)ethyl)-1*H*-pyrazol-1-yl)-3-((2-(trimethylsilyl)ethoxy)methyl)pyrido[3,4-*d*]pyrimidin-4(3*H*)-one (274 mg, 0.546 mmol, 1 equiv) in MeOH (5.5 mL, 0.1 M) at 0 °C. The reaction was stirred at 0 °C for 5 min, then diluted with EtOAc (20 mL), washed with saturated $NaHCO_3$ solution (20 mL) and saturated brine solution (20 mL), dried over $MgSO_4$, and concentrated in vacuo to give

the product as a white solid (210 mg, 99%). ¹H NMR (500 MHz, $CDCl_3$) δ 0.01 (s, 9H), 0.96–1.00 (m, 2H), 2.86 (t, *J* = 6.3 Hz, 2H), 3.67–3.72 (m, 2H), 3.88 (t, *J* = 6.3 Hz, 2H), 5.46 (s, 2H), 7.81 (s, 1H), 8.07 (d, *J* = 5.1 Hz, 1H), 8.30 (s, 1H), 8.60 (s, 1H), 8.62 (d, *J* = 5.1 Hz, 1H), OH signal not observed. LC-MS (method H; ESI, *m/z*) *t*_R = 1.34 min –388 [(*M* + H)⁺]. HRMS (method I): found, 388.1798; calculated for $C_{18}H_{26}N_5O_3Si$ ($M + H$)⁺, 388.1805.

8-(4-(2-((4-Fluorobenzyl) (methyl)amino)ethyl)-1*H*-pyrazol-1-yl)-3-((2-(trimethylsilyl)ethoxy)methyl)pyrido[3,4-*d*]pyrimidin-4(3*H*)-one (49d). Methanesulfonic anhydride (94 mg, 0.542 mmol, 1.5 equiv) was added in one portion to a solution of alcohol 47 (140 mg, 0.361 mmol, 1 equiv) and triethylamine (0.1 mL, 0.717 mmol, 2 equiv) in anhydrous CH_2Cl_2 (4 mL, 0.09 M) at 0 °C under N_2 . The reaction mixture was stirred for 15 min at 0 °C and monitored by LCMS. When the reaction was complete, the reaction mixture was quenched with saturated $NaHCO_3$ (10 mL) solution and extracted with CH_2Cl_2 (3 × 15 mL). The combined organic layers were washed with saturated brine solution (30 mL), dried over $MgSO_4$, and concentrated in vacuo to give 2-(1-(4-oxo-3-((2-(trimethylsilyl)ethoxy)methyl)-3,4-dihydropyrido[3,4-*d*]pyrimidin-8-yl)-1*H*-pyrazol-4-yl)ethylmethanesulfonate as a pale-yellow oil. This was used in the next step without further purification. ¹H NMR (500 MHz, $CDCl_3$) δ 0.01 (s, 9H), 0.96–1.01 (m, 2H), 2.99 (s, 3H), 3.07 (t, *J* = 6.7 Hz, 2H), 3.68–3.72 (m, 2H), 4.44 (t, *J* = 6.7 Hz, 2H), 5.47 (s, 2H), 7.81 (s, 1H), 8.09 (d, *J* = 5.1 Hz, 1H), 8.31 (s, 1H), 8.64 (d, *J* = 5.1 Hz, 1H), 8.68 (s, 1H). LC-MS (method H; ESI, *m/z*) *t*_R = 1.34 min –466 [(*M* + H)⁺]. According to general procedure 1, cesium carbonate (340 mg, 1.044 mmol), 2-(1-(4-oxo-3-((2-(trimethylsilyl)ethoxy)methyl)-3,4-dihydropyrido[3,4-*d*]pyrimidin-8-yl)-1*H*-pyrazol-4-yl)ethylmethanesulfonate (162 mg, 0.348 mmol), and 1-(4-fluorophenyl)-*N*-methylmethanamine (0.1 mL, 0.759 mmol) were reacted together in anhydrous DMF (2 mL). Purification on a KP-Sil snap cartridge (2% EtOH in CH_2Cl_2) gave the title product as a pale-yellow oil (27.7 mg, 29%). ¹H NMR (500 MHz, $CDCl_3$) δ 0.01 (s, 9H), 0.95–1.01 (m, 2H), 2.28 (s, 3H), 2.69 (t, *J* = 7.4 Hz, 2H), 2.80 (t, *J* = 7.4 Hz, 2H), 3.54 (s, 2H), 3.68–3.72 (m, 2H), 5.47 (s, 2H), 6.96–7.01 (m, 2H), 7.28–7.31 (m, 2H), 7.78 (s, 1H), 8.06 (d, *J* = 5.1 Hz, 1H), 8.30 (s, 1H), 8.54 (s, 1H), 8.63 (d, *J* = 5.1 Hz, 1H). LC-MS (method C; ESI, *m/z*) *t*_R = 1.19 min –509 [(*M* + H)⁺]. HRMS (method B): found, 509.2514; calculated for $C_{26}H_{34}FN_6O_2Si$ ($M + H$)⁺, 509.2496.

8-(4-(2-((4-Fluorobenzyl) (methyl)amino)ethyl)-1*H*-pyrazol-1-yl)pyrido[3,4-*d*]pyrimidin-4(3*H*)-one (52d). According to general procedure 4, 8-(4-(2-((4-fluorobenzyl) (methyl)amino)ethyl)-1*H*-pyrazol-1-yl)-3-((2-(trimethylsilyl)ethoxy)methyl)-pyrido[3,4-*d*]pyrimidin-4(3*H*)-one (42.46 mg, 0.083 mmol) and hydrochloric acid (6 M, 1 mL) were reacted together in THF (1 mL). Purification on a KP-NH snap cartridge (25% EtOH in CH_2Cl_2) gave the product as a white solid (23.6 mg, 75%). ¹H NMR (500 MHz, MeOH-*d*₄) δ 2.35 (s, 3H), 2.73–2.78 (m, 2H), 2.83–2.88 (m, 2H), 3.66 (s, 2H), 7.02–7.08 (m, 2H), 7.34–7.39 (m, 2H), 7.75 (s, 1H), 8.04 (d, *J* = 5.2 Hz, 1H), 8.23 (s, 1H), 8.55 (d, *J* = 5.2 Hz, 1H), 8.70 (s, 1H), NH signal not observed. LC-MS (method C; ESI, *m/z*) *t*_R = 0.68 min –379 [(*M* + H)⁺]. HRMS (method B): found, 379.1665; calculated for $C_{20}H_{20}FN_6O$ ($M + H$)⁺, 379.1677.

8-(4-(2-(4-(4-Chlorophenyl)piperidin-1-yl)ethyl)-1*H*-pyrazol-1-yl)-3-((2-(trimethylsilyl)ethoxy)methyl)pyrido[3,4-*d*]pyrimidin-4(3*H*)-one (51a). According to general procedure 2, 2-(1-(4-oxo-3-((2-(trimethylsilyl)ethoxy)methyl)-3,4-dihydropyrido[3,4-*d*]pyrimidin-8-yl)-1*H*-pyrazol-4-yl)ethylmethanesulfonate (96 mg, 0.206 mmol), 4-(4-chlorophenyl)piperidine (48 mg, 0.247 mmol), and triethylamine (0.057 mL, 0.409 mmol) in DMF were reacted at 50 °C overnight. After workup, the resulting oil was passed through a plug of silica eluting with 30% MeOH/DCM to afford a yellow oil which was used without further purification. ¹H NMR (500 MHz, $CDCl_3$) δ 0.01 (s, 9H), 0.96–1.02 (m, 2H), 1.75–1.90 (m, 4H), 2.12–2.19 (m, 2H), 2.48–2.57 (m, 1H), 2.67–2.73 (m, 2H), 2.81–2.86 (m, 2H), 3.14 (br s, 1H), 3.16 (br s, 1H), 3.68–3.73 (m, 2H), 5.47 (s, 2H), 7.11 (d, *J* = 8.4 Hz, 2H), 7.18 (d, *J* = 8.4 Hz, 2H), 7.80 (s, 1H), 8.08 (d, *J* = 5.1 Hz, 1H), 8.30 (s, 1H), 8.57 (s, 1H), 8.64 (d, *J* = 5.1 Hz, 1H). LC-HRMS (method C) *t*_R = 1.28 min, *m/z* –565.2515 Cl isotopic pattern [(*M* + H)⁺].

8-(4-(2-(4-(4-Chlorophenyl)piperidin-1-yl)ethyl)-1H-pyrazol-1-yl)pyrido[3,4-d]pyrimidin-4(3H)-one (54a). According to general procedure 5, 8-(4-(2-(4-(4-chlorophenyl)piperidin-1-yl)ethyl)-1H-pyrazol-1-yl)-3-((2-(trimethylsilyl)ethoxy)methyl)-pyrido[3,4-d]pyrimidin-4(3H)-one (73 mg, 0.129 mmol) was reacted with HCl in 1,4-dioxane (4 M, 0.81 mL, 3.23 mmol) in 1,4-dioxane/water at 50 °C overnight. After workup and trituration, the title product was obtained (16 mg, 29%) as an off-white solid. ¹H NMR (500 MHz, DMSO-*d*₆) δ 1.65 (qd, *J* = 12.3, 3.5 Hz, 2H), 1.76 (d, *J* = 11.2 Hz, 2H), 2.11 (t, *J* = 7.5 Hz, 2H), 2.53–2.65 (m, 3H), 2.72 (t, *J* = 7.5 Hz, 2H), 3.09 (d, *J* = 11.2 Hz, 2H), 7.29 (d, *J* = 8.3 Hz, 2H), 7.34 (d, *J* = 8.3 Hz, 2H), 7.73 (s, 1H), 7.98 (d, *J* = 5.1 Hz, 1H), 8.29 (s, 1H), 8.42 (s, 1H), 8.56 (d, *J* = 5.1 Hz, 1H), 12.44 (br s, 1H). LC-HRMS (method I) *t*_R = 2.01 min, *m/z* found, 435.1696; calculated for C₂₃H₂₄ClN₆O [(M + H)⁺], 435.1700 Cl isotopic pattern.

8-(4-(2-(4-(3,5-Dichlorophenyl)piperidin-1-yl)ethyl)-1H-pyrazol-1-yl)-3-((2-(trimethylsilyl)ethoxy)methyl)pyrido[3,4-d]pyrimidin-4(3H)-one (51j). According to general procedure 2, triethylamine (0.06 mL, 0.411 mmol), 2-(1-(4-oxo-3-((2-(trimethylsilyl)ethoxy)methyl)-3,4-dihydropyrido[3,4-d]pyrimidin-8-yl)-1H-pyrazol-4-yl)ethylmethanesulfonate (95.7 mg, 0.206 mmol), and 4-(3,5-dichlorophenyl)piperidine (95 mg, 0.411 mmol) were reacted together in anhydrous DMF (1 mL) and purified on KP-Sil snap cartridge (4% [0.2 M NH₃ in MeOH] in CH₂Cl₂) to give the product as a pale-yellow oil (104 mg, 84%). ¹H NMR (500 MHz, CDCl₃) δ 0.00 (s, 9H), 0.95–1.00 (m, 2H), 1.78 (qd, *J* = 12.0, 3.1 Hz, 2H), 1.83–1.89 (m, 2H), 2.14 (td, *J* = 11.8, 1.9 Hz, 2H), 2.45–2.54 (m, 1H), 2.66–2.71 (m, 2H), 2.79–2.85 (m, 2H), 3.14 (br d, *J* = 11.4 Hz, 2H), 3.66–3.72 (m, 2H), 5.46 (s, 2H), 7.11 (d, *J* = 1.9 Hz, 2H), 7.19 (t, *J* = 1.9 Hz, 1H), 7.80 (s, 1H), 8.06 (d, *J* = 5.1 Hz, 1H), 8.30 (s, 1H), 8.57 (s, 1H), 8.62 (d, *J* = 5.1 Hz, 1H). LC-MS (method H; ESI, *m/z*) *t*_R = 1.32 min –599, 601, 603 [(M + H)⁺, Cl isotopic pattern]. HRMS (method I): found, 599.2128; calculated for C₂₉H₃₇Cl₂N₆O₂Si (M + H)⁺, 599.2124.

8-(4-(2-(4-(3,5-Dichlorophenyl)piperidin-1-yl)ethyl)-1H-pyrazol-1-yl)pyrido[3,4-d]pyrimidin-4(3H)-one (54j). According to general procedure 4, 8-(4-(2-(4-(3,5-dichlorophenyl)piperidin-1-yl)ethyl)-1H-pyrazol-1-yl)-3-((2-(trimethylsilyl)ethoxy)methyl)-pyrido[3,4-d]pyrimidin-4(3H)-one (40.6 mg, 0.068 mmol) and hydrochloric acid (6 M, 1 mL) were reacted together in THF (1 mL). Purification on a KP-NH snap cartridge (40% EtOH in CH₂Cl₂) gave the product as a white solid (16.4 mg, 52%). ¹H NMR (500 MHz, DMSO-*d*₆) δ 1.66 (qd, *J* = 12.4, 3.5 Hz, 2H), 1.73–1.80 (m, 2H), 2.06 (t, *J* = 11.6, 1.6 Hz, 2H), 2.54–2.61 (m, 3H), 2.71 (t, *J* = 7.5 Hz, 2H), 3.06 (br d, *J* = 11.3 Hz, 2H), 7.33 (d, *J* = 1.9 Hz, 2H), 7.41 (t, *J* = 1.9 Hz, 1H), 7.73 (s, 1H), 7.98 (d, *J* = 5.1 Hz, 1H), 8.29 (s, 1H), 8.41 (s, 1H), 8.55 (d, *J* = 5.1 Hz, 1H) 12.79 (br s, 1H). LC-MS (method H; ESI, *m/z*) *t*_R = 1.02 min –469, 471, 473 [(M + H)⁺, Cl isotopic pattern]. HRMS (method I): found, 469.1316; calculated for C₂₃H₂₃Cl₂N₆O (M + H)⁺, 469.1310.

8-(4-(2-(4-(3-Chlorophenyl)piperidin-1-yl)ethyl)-1H-pyrazol-1-yl)-3-((2-(trimethylsilyl)ethoxy)methyl)pyrido[3,4-d]pyrimidin-4(3H)-one (51k). According to general procedure 2, 2-(1-(4-oxo-3-((2-(trimethylsilyl)ethoxy)methyl)-3,4-dihydropyrido[3,4-d]pyrimidin-8-yl)-1H-pyrazol-4-yl)ethylmethanesulfonate (79 mg, 0.170 mmol), 4-(3-chlorophenyl)piperidine hydrochloride (59 mg, 0.255 mmol), and triethylamine (0.057 mL, 0.409 mmol) in DMF were reacted at 50 °C for 3 days. After workup, the oil obtained was purified by flash column chromatography to afford the product (23 mg, 24%) as a yellow oil. ¹H NMR (500 MHz, CDCl₃) δ 0.02 (s, 9H), 0.96–1.01 (m, 2H), 1.81–1.93 (m, 5H), 2.15–2.24 (m, 2H), 2.49–2.60 (m, 1H), 2.69–2.77 (m, 2H), 2.83–2.91 (m, 2H), 3.15–3.21 (m, 2H), 3.67–3.73 (m, 2H), 5.48 (s, 2H), 7.12–7.15 (m, 1H), 7.17–7.20 (m, 1H), 7.23–7.27 (m, 1H), 7.81 (br s, 1H), 8.08 (d, *J* = 5.1 Hz, 1H), 8.32 (s, 1H), 8.59 (br s, 1H), 8.64 (br s, 1H). LC-HRMS (method I) *t*_R = 2.80 min. HRMS: found, 565.2480; calculated for C₂₉H₃₈ClN₆O₂Si [(M + H)⁺], 565.2514 Cl isotopic pattern.

8-(4-(2-(4-(3-Chlorophenyl)piperidin-1-yl)ethyl)-1H-pyrazol-1-yl)pyrido[3,4-d]pyrimidin-4(3H)-one (54k). According to general procedure 5, 8-(4-(2-(4-(3-chlorophenyl)piperidin-1-yl)ethyl)-1H-pyrazol-1-yl)-3-((2-(trimethylsilyl)ethoxy)methyl)-pyrido[3,4-d]pyrimidin-4(3H)-one (23 mg, 0.041 mmol) was reacted with HCl in

1,4-dioxane (4M, 0.1 mL, 0.407 mmol) in 1,4-dioxane/water at 50 °C overnight. After workup and trituration with Et₂O, the title product was obtained (9 mg, 51%) as a yellow solid. ¹H NMR (500 MHz, DMSO-*d*₆) δ 1.66 (dq, *J* = 12.3, 3.5 Hz, 2H), 1.76 (br s, 1H), 1.78 (br s, 1H), 2.09 (t, *J* = 10.4 Hz, 2H), 2.53–2.57 (m, 1H), 2.60 (t, *J* = 7.3 Hz, 2H), 2.72 (t, *J* = 7.3 Hz, 2H), 3.04–3.10 (m, 2H), 7.22–7.26 (m, 2H), 7.30–7.35 (m, 2H), 7.73 (s, 1H), 7.98 (d, *J* = 5.3 Hz, 1H), 8.29 (s, 1H), 8.42 (s, 1H), 8.56 (d, *J* = 5.3 Hz, 1H), 12.78 (br s, 1H). LC-HRMS (method I) *t*_R = 2.14 min. HRMS: found, 435.1675; calculated for C₂₃H₂₄ClN₆O [(M + H)⁺], 435.1695.

■ ASSOCIATED CONTENT

Supporting Information

The Supporting Information is available free of charge on the ACS Publications website at DOI: 10.1021/acs.jmedchem.5b01635.

Experimental procedures for compounds 7a,b,d, 9a,b, 16, 21, 22, 24, 25, 17–19, 27, 28, 29a,b, 30a,b, 36–40, 41a,b, 42, 43, 44a–g, 48, 55–57, 49a–c, 49e–g, 52a–c, 52e–g, 59, and intermediates for the synthesis of 59, 50a–i, 53a–i, 51b–i, 51l–n, 54b–i, and 54l–n, a summary of crystallographic analysis of compounds 15, 16, 30a, 30b, 37, 40, 52d, 53a, 54a, 54j, and 58, kinase profiling for compound 54k, and cellular activity of 54k in HeLa cells assessed by immunofluorescence assay (PDF)

Molecular formula strings (CSV)

Accession Codes

Atomic coordinates and structure factors for the crystal structures of KDM4A with compounds 15, 16, 30b, 37, 40, 52d, 53a, 54a, 54j, and 58 can be accessed using PDB codes SF2S, SF2W, SF5I, SF39, SF32, SF3C, SF3G, SF3E, SF3I, and SF37, respectively. Atomic coordinates and structure factors for the crystal structures of KDM4D with compounds 30a and 44a can be accessed using PDB codes SF5A and SF5C, respectively. Atomic coordinates and structure factors for the crystal structures of KDM5B with compound 52d can be accessed using PDB code SFPI.

■ AUTHOR INFORMATION

Corresponding Authors

*For V.B.: phone, +44 (0) 20 87224158; E-mail, vassilios.bavetsias@icr.ac.uk.

*For P.E.B.: phone, +44 (0) 1865 612932; E-mail, paul.brennan@sgc.ox.ac.uk.

*For J.B.: phone, +44 (0) 20 87224051; E-mail, julian.blagg@icr.ac.uk.

Notes

The authors declare no competing financial interest.

■ ACKNOWLEDGMENTS

This work was supported by Cancer Research UK [CUK] grant no. C309/A11566. We thank the Avon Foundation for Women for funding (Gift Agreement grant no. 02-2013-52), and we thank Dr. Stephen H. Friend MD Ph.D. of Sage Bionetworks for his support. The SGC is a registered charity (no. 1097737) that receives funds from AbbVie, Bayer Pharma AG, Boehringer Ingelheim, Canada Foundation for Innovation, Eshelman Institute for Innovation, Genome Canada, Innovative Medicines Initiative (EU/EFPIA) [ULTRA-DD grant no. 115766], Janssen, Merck & Co., Novartis Pharma AG, Ontario Ministry of Economic Development and Innovation, Pfizer, São Paulo Research Foundation-FAPESP, Takeda, and Wellcome Trust [092809/Z/10/Z]. We acknowledge NHS funding to the NIHR Biomedical Research Centre at The Institute of Cancer Research

and the Royal Marsden NHS Foundation Trust. We thank Dr. Amin Mirza, Meirion Richards, and Dr. Maggie Liu for their assistance with NMR, mass spectrometry, and HPLC. We thank Dr Nora Cronin and the staff of DIAMOND Light Source and European Synchrotron Radiation Facility for their support during crystallographic data collection.

ABBREVIATIONS USED

Boc, *tert*-butoxycarbonyl; DME, 1,2-dimethoxyethane; DIBAL, diisobutylaluminum hydride; EDCI, *N*-(3-(dimethylamino)propyl)-*N'*-ethylcarbodiimide hydrochloride; ESI, electrospray ionization; HPLC, high performance liquid chromatography; HOBt, 1-hydroxybenzotriazole; HRMS, high resolution mass spectrometry; JmjC, Jumonji C; LC, liquid chromatography; LE, ligand efficiency; LSD, lysine specific demethylase; NOG, *N*-oxalylglycine; 2OG, 2-oxoglutarate; PTSA, *p*-toluenesulfonic acid; PDB, Protein Data Bank; SAR, structure–activity relationship; SEM, 2-(trimethylsilyl)ethoxymethyl; TFA, trifluoroacetic acid

REFERENCES

- (1) Pedersen, M. T.; Helin, K. Histone Demethylases in Development and Disease. *Trends Cell Biol.* **2010**, *20*, 662–671.
- (2) Shi, Y.; Whetstone, J. R. Dynamic Regulation of Histone Lysine Methylation by Demethylases. *Mol. Cell* **2007**, *25*, 1–14.
- (3) Shiau, C.; Trnka, M. J.; Bozicevic, A.; Torres, I. O.; Al-Sady, B.; Burlingame, A. L.; Narlikar, G. J.; Fujimori, D. G. Reconstitution of Nucleosome Demethylation and Catalytic Properties of a Jumonji Histone Demethylase. *Chem. Biol.* **2013**, *20*, 494–499.
- (4) Kooistra, S. M.; Helin, K. Molecular Mechanisms and Potential Functions of Histone Demethylases. *Nat. Rev. Mol. Cell Biol.* **2012**, *13*, 297–311.
- (5) Young, L. C.; Hendzel, M. J. The Oncogenic Potential of Jumonji D2 (JMJD2/KDM4) Histone Demethylase Overexpression. *Biochem. Cell Biol.* **2013**, *91*, 369–377.
- (6) Hillringhaus, L.; Yue, W. W.; Rose, N. R.; Ng, S. S.; Gileadi, C.; Loenarz, C.; Bello, S. H.; Bray, J. E.; Schofield, C. J.; Oppermann, U. Structural and Evolutionary Basis for the Dual Substrate Selectivity of Human KDM4 Histone Demethylase Family. *J. Biol. Chem.* **2011**, *286*, 41616–41625.
- (7) Berry, W. L.; Janknecht, R. KDM4/JMJD2 Histone Demethylases: Epigenetic Regulators in Cancer Cells. *Cancer Res.* **2013**, *73*, 2936–2942.
- (8) Williams, S. T.; Walport, L. J.; Hopkinson, R. J.; Madden, S. K.; Chowdhury, R.; Schofield, C. J.; Kawamura, A. Studies on the Catalytic Domains of Multiple JmjC Oxygenases Using Peptide Substrates. *Epigenetics* **2014**, *9*, 1596–1603.
- (9) Trojer, P.; Zhang, J.; Yonezawa, M.; Schmidt, A.; Zheng, H.; Jenuwein, T.; Reinberg, D. Dynamic Histone H1 Isoform 4 Methylation and Demethylation by Histone Lysine Methyltransferase G9a/KMT1C and the Jumonji Domain-containing JMJ/KDM4 Proteins. *J. Biol. Chem.* **2009**, *284*, 8395–8405.
- (10) Liu, G.; Bollig-Fischer, A.; Kreike, B.; van de Vijver, M. J.; Abrams, J.; Ethier, S. P.; Yang, Z.-Q. Genomic Amplification and Oncogenic Properties of the GASC1 Histone Demethylases Gene in Breast Cancer. *Oncogene* **2009**, *28*, 4491–4500.
- (11) Kawazu, M.; Saso, K.; Tong, K. I.; McQuire, T.; Goto, K.; Son, D.-O.; Wakeham, A.; Miyagishi, M.; Mak, T. W.; Okada, H. Histone Demethylase JMJD2B Functions as a Co-Factor of Estrogen Receptor in Breast Cancer Proliferation and Mammary Gland Development. *PLoS One* **2011**, *6*, e17830.
- (12) Li, W.; Zhao, L.; Zang, W.; Liu, Z.; Chen, L.; Liu, T.; Xu, D.; Jia, J. Histone Demethylase JMJD2B is Required for Tumour Cell Proliferation and Survival and is Overexpressed in Gastric Cancer. *Biochem. Biophys. Res. Commun.* **2011**, *416*, 372–378.
- (13) Walters, Z. S.; Villarejo-Balcells, B.; Olmos, D.; Buist, T. W. S.; Missiaglia, E.; Allen, R.; Al-Lazikani, B.; Garrett, M. D.; Blagg, J.; Shipley, J. JARID2 is a Direct Target of the PAX3-FOXO1 Fusion Protein and Inhibits Myogenic Differentiation of Rhabdomyosarcoma Cells. *Oncogene* **2014**, *33*, 1148–1157.
- (14) Yang, J.; Al Tahan, A. M.; Hu, D.; Wang, Y.; Cheng, P.-H.; Morton, C. L.; Qu, C.; Nathwani, A. C.; Shohet, J. M.; Fotsis, T.; Koster, J.; Versteeg, R.; Okada, H.; Harris, A. L.; Davidoff, A. M. The Role of Histone Demethylase KDM4B in Myc Signaling in Neuroblastoma. *J. Natl. Cancer Inst.* **2015**, *107*, djv080.
- (15) Black, J. C.; Manning, A. L.; Van Rechem, C.; Kim, J.; Ladd, B.; Cho, J.; Pineda, C. M.; Murphy, N.; Daniels, D. L.; Montagna, C.; Lewis, P. W.; Glass, K.; Allis, D. C.; Dyson, N. J.; Getz, G.; Whetstone, J. R. KDM4A Lysine Demethylase Induces Site-Specific Copy Gain and Rereplication of Regions Amplified in Tumors. *Cell* **2013**, *154*, 541–555.
- (16) Van Rechem, C.; Black, J. C.; Greninger, P.; Zhao, Y.; Donado, C.; Burrows, P. D.; Ladd, B.; Christiani, D. C.; Benes, C. H.; Whetstone, J. R. A Coding Single-Nucleotide Polymorphism in Lysine Demethylase KDM4A Associates with Increased Sensitivity to mTOR Inhibitors. *Cancer Discovery* **2015**, *5*, 245–254.
- (17) Van Rechem, C.; Black, J. C.; Boukhalil, M.; Aryee, M. J.; Graslund, S.; Haas, W.; Benes, C. H.; Whetstone, J. R. Lysine Demethylase KDM4A Associates with Translation Machinery and Regulates Protein Synthesis. *Cancer Discovery* **2015**, *5*, 255–263.
- (18) Blair, L. P.; Cao, J.; Zou, M. R.; Sayegh, J.; Yan, Q. Epigenetic Regulation by Lysine Demethylase 5 (KDM5) Enzymes in Cancer. *Cancers* **2011**, *3*, 1383–1404.
- (19) You, J. S.; Jones, P. A. Cancer Genetics and Epigenetics: Two Sides of the Same Coin? *Cancer Cell* **2012**, *22*, 9–20.
- (20) Klein, B. J.; Piao, L.; Xi, Y.; Rincon-Arango, H.; Rothbart, S. B.; Peng, D.; Wen, H.; Larson, C.; Zhang, X.; Zheng, X.; Cortazar, M. A.; Pena, P. V.; Mangan, A.; Bentley, D. L.; Strahl, B. D.; Groudine, M.; Li, W.; Shi, X.; Kutateladze, T. G. The Histone-H3K4-specific Demethylase KDM5B Binds to Its Substrate and Product Through Distinct PHD Fingers. *Cell Rep.* **2014**, *6*, 325–335.
- (21) Yamamoto, S.; Wu, Z.; Russnes, H. G.; Takagi, S.; Peluffo, G.; Vaske, C.; Zhao, X.; Moen Volla, H. K.; Maruyama, R.; Ekram, M. B.; Sun, H.; Kim, J. H.; Carver, K.; Zucca, M.; Feng, J.; Almendro, V.; Bessarabova, M.; Rueda, O. M.; Nikolsky, Y.; Caldas, C.; Liu, X. S.; Polyak, K. JARID1B Is a Luminal Lineage-Driving Oncogene in Breast Cancer. *Cancer Cell* **2014**, *25*, 762–777.
- (22) Stein, J.; Majores, M.; Rohde, M.; Lim, S.; Schneider, S.; Krappe, E.; Ellinger, J.; Dietel, M.; Stephan, C.; Jung, K.; Perner, S.; Kristiansen, G.; Kirfel, J. KDM5C Is Overexpressed in Prostate Cancer and Is a Prognostic Marker for Prostate-Specific Antigen-Relapse Following Radical Prostatectomy. *Am. J. Pathol.* **2014**, *184*, 2430–2437.
- (23) Helin, K.; Dhanak, D. Chromatin Proteins and Modifications as Drug Targets. *Nature* **2013**, *502*, 480–488.
- (24) Kruidenier, L.; Chung, C.-W.; Cheng, Z.; Liddle, J.; Che, K.; Joberty, G.; Bantscheff, M.; Bountra, C.; Bridges, A.; Diallo, H.; Eberhard, D.; Hutchinson, S.; Jones, E.; Katso, R.; Leveridge, M.; Mander, P. K.; Mosley, J.; Ramirez-Molina, C.; Rowland, P.; Schofield, C. J.; Sheppard, R. J.; Smith, J. E.; Swales, C.; Tanner, R.; Thomas, P.; Tumber, A.; Drewes, G.; Oppermann, U.; Patel, D. J.; Lee, K.; Wilson, D. M. A Selective Jumonji H3K27 Demethylase Inhibitor Modulates the Proinflammatory Macrophage Response. *Nature* **2012**, *488*, 404–408.
- (25) Labbe, R. M.; Holowatyj, A.; Yang, Z.-Q. Histone Lysine Demethylase (KDM) Subfamily 4: Structures, Functions and Therapeutic Potential. *Am. J. Transl. Res.* **2014**, *6*, 1–15.
- (26) Heightman, T. D. Chemical Biology of Lysine Demethylases. *Curr. Chem. Genomics* **2011**, *5*, 62–71.
- (27) Suzuki, T.; Miyata, N. Lysine Demethylases Inhibitors. *J. Med. Chem.* **2011**, *54*, 8236–8250.
- (28) Lohse, B.; Kristensen, J. L.; Kristensen, L. H.; Agger, K.; Helin, K.; Gajhede, M.; Clausen, R. P. Inhibitors of Histone Demethylases. *Bioorg. Med. Chem.* **2011**, *19*, 3625–3636.
- (29) Hoffmann, I.; Roatsch, M.; Schmitt, M. L.; Carlino, L.; Pippel, M.; Sippl, W.; Jung, M. The Role of Histone Demethylases in Cancer Therapy. *Mol. Oncol.* **2012**, *6*, 683–703.

- (30) Zheng, W.; Huang, Y. The Chemistry and Biology of the α -Ketoglutarate-Dependent Histone N^{ϵ} -Methyl-Lysine Demethylases. *Med. MedChemComm* **2014**, *5*, 297–313.
- (31) Chin, Y.-W.; Han, S.-Y. KDM4 Histone Demethylase Inhibitors for Anti-cancer Agents: A Patent Review. *Expert Opin. Ther. Pat.* **2015**, *25*, 135–144.
- (32) Rose, N. R.; Ng, S. S.; Mecinovic, J.; Lienard, B. M. R.; Bello, S. H.; Sun, Z.; McDonough, M. A.; Oppermann, U.; Schofield, C. J. Inhibitor Scaffolds for 2-Oxoglutarate-Dependent Histone Lysine Demethylases. *J. Med. Chem.* **2008**, *51*, 7053–7056.
- (33) Chang, K.-H.; King, O. N. F.; Tumber, A.; Woon, E. C. Y.; Heightman, T. D.; McDonough, M. A.; Schofield, C. J.; Rose, N. R. Inhibition of Histone Demethylases by 4-Carboxy-2,2' - Bipyridyl Compounds. *ChemMedChem* **2011**, *6*, 759–764.
- (34) England, K. S.; Tumber, A.; Krojer, T.; Scozzafava, G.; Ng, S. S.; Daniel, M.; Szykowska, A.; Che, K.; von Delft, F.; Burgess-Brown, N. A.; Kawamura, A.; Schofield, C. J.; Brennan, P. E. Optimisation of a Triazolopyridine Based Histone Demethylase Inhibitor Yields a Potent and Selective KDM2A (FBXL11) Inhibitor. *MedChemComm* **2014**, *5*, 1879–1886.
- (35) Mjambili, F.; Njoroge, M.; Naran, K.; De Kock, C.; Smith, P. J.; Mizrahi, V.; Warner, D.; Chibale, K. Synthesis and Biological Evaluation of 2-Aminothiazole Derivatives as Antimycobacterial and Antiplasmodial Agents. *Bioorg. Med. Chem. Lett.* **2014**, *24*, 560–564.
- (36) Labelle, M.; Boesen, T.; Mehrotra, M.; Khan, Q.; Ullah, F. Inhibitors of Histone Demethylases. WO2014/053491, 2014.
- (37) Ng, S. S.; Kavanagh, K. L.; McDonough, M. A.; Butler, D.; Pilka, E. S.; Lienard, B. M. R.; Bray, J. E.; Savitsky, P.; Gileadi, O.; von Delft, F.; Rose, N. R.; Offer, J.; Scheinost, J. C.; Borowski, T.; Sundstrom, M.; Schofield, C. J.; Oppermann, U. Crystal Structures of Histone Demethylase JMJD2A Reveal Basis for Substrate Specificity. *Nature* **2007**, *448*, 87–91.
- (38) Chu, C.-H.; Wang, L.-Y.; Hsu, K.-S.; Chen, C.-C.; Cheng, H.-H.; Wang, S.-M.; Wu, C.-M.; Chen, T.-J.; Li, L.-T.; Liu, R.; Hung, C.-L.; Yang, J.-M.; Kung, H.-J.; Wang, W.-C. KDM4B as a Target for Prostate Cancer: Structural Analysis and Selective Inhibition by a Novel Inhibitor. *J. Med. Chem.* **2014**, *57*, 5975–5985.
- (39) Personal communication from Susan Westaway and Jack Brown, GlaxoSmithKline. See also: Cell Penetrant Inhibitors of the KDM4 and KDM5 Families of Histone Lysine Demethylases. Part 2: Pyrido[3,4-*d*]pyrimidin-4(3H)-one derivatives, this issue of *J. Med. Chem.*, DOI: [10.1021/acs.jmedchem.5b01538](https://doi.org/10.1021/acs.jmedchem.5b01538).
- (40) Kanouni, T.; Stafford, J. A.; Veal, J. M.; Wallace, M. B. Histone Demethylase Inhibitors. WO2014/151106, 2014.
- (41) pK_a Measurements were performed by Pharmorphix Solid State Services, Member of the Sigma-Aldrich Group, Cambridge, UK (Currently known as: Johnson Matthey Plc, Fine Chemicals Division (Pharmorphix), Cambridge, UK).
- (42) Pryde, D. C.; Dalvie, D.; Hu, Q.; Jones, P.; Obach, R. S.; Tran, T.-D. Aldehyde Oxidase: An Enzyme of Emerging Importance in Drug Discovery. *J. Med. Chem.* **2010**, *53*, 8441–8460.
- (43) A full account on metabolite identification and strategies to block AO-mediated metabolism in this series will be reported elsewhere.
- (44) Kinase selectivity profiling for compound **54k** was carried out at the International Centre for Kinase Profiling, Division of Signal Transduction Therapy, College of Life Sciences, University of Dundee, UK.
- (45) Hopkinson, R. J.; Tumber, A.; Yapp, C.; Chowdhury, R.; Aik, W.; Che, K. H.; Li, X. S.; Kristensen, J. B. L.; King, O. N. F.; Chan, M. C.; Yeoh, K. H.; Choi, H.; Walport, L. J.; Thinnes, C. C.; Bush, J. T.; Lejeune, C.; Rydzik, A. M.; Rose, N. R.; Bagg, E. A.; McDonough, M. A.; Krojer, T. J.; Yue, W. W.; Ng, S. S.; Olsen, L.; Brennan, P. E.; Oppermann, U.; Müller, S.; Klose, R. J.; Ratcliffe, P. J.; Schofield, C. J.; Kawamura, A. 5-Carboxy-8-Hydroxyquinoline is a Broad Spectrum 2-Oxoglutarate Oxygenase Inhibitor Which Causes Iron Translocation. *Chem. Sci.* **2013**, *4*, 3110–3117.
- (46) Kawamura, A.; Tumber, A.; Rose, N. R.; King, O. N. F.; Daniel, M.; Oppermann, U.; Heightman, T. D.; Schofield, C. Development of Homogeneous Luminescence Assays for Histone Demethylase Catalysis and Binding. *Anal. Biochem.* **2010**, *404*, 86–93.
- (47) *Maestro*, version 9.3; Schrödinger, LLC: New York, 2012.
- (48) *Glide*, version 5.8; Schrödinger, LLC: New York, 2012.
- (49) *LigPrep*, version 2.5; Schrödinger, LLC: New York, 2011.
- (50) Savitsky, P.; Bray, J.; Cooper, C. D.; Marsden, B. D.; Mahajan, P.; Burgess-Brown, N. A.; Gileadi, O. High-throughput Production of Human Proteins for Crystallization: The SGC Experience. *J. Struct. Biol.* **2010**, *172*, 3–13.
- (51) Kabsch, W. XDS. *Acta Crystallogr., Sect. D: Biol. Crystallogr.* **2010**, *66*, 125–132.
- (52) Evans, P. Scaling and Assessment of Data Quality. *Acta Crystallogr., Sect. D: Biol. Crystallogr.* **2006**, *62*, 72–82.
- (53) McCoy, A. J.; Grosse-Kunstleve, R. W.; Adams, P. D.; Winn, M. D.; Storoni, L. C.; Read, R. J. Phaser Crystallographic Software. *J. Appl. Crystallogr.* **2007**, *40*, 658–674.
- (54) Winn, M. D.; Ballard, C. C.; Cowtan, K. D.; Dodson, E. J.; Emsley, P.; Evans, P. R.; Keegan, R. M.; Krissinel, E. B.; Leslie, A. G.; McCoy, A.; McNicholas, S. J.; Murshudov, G. N.; Pannu, N. S.; Potterton, E. A.; Powell, H. R.; Read, R. J.; Vagin, A.; Wilson, K. S. Overview of the CCP4 Suite and Current Developments. *Acta Crystallogr., Sect. D: Biol. Crystallogr.* **2011**, *67*, 235–242.
- (55) Emsley, P.; Cowtan, K. Coot: Model-building Tools for Molecular Graphics. *Acta Crystallogr., Sect. D: Biol. Crystallogr.* **2004**, *60*, 2126–2132.
- (56) Bricogne, G.; Blanc, E.; Brandl, M.; Flensburg, C.; Keller, P.; Paciorek, W.; Roversi, P.; Sharff, A.; Smart, O. S.; Vonnrhein, C.; Womack, T. O. *BUSTER*, version 2.10.2; Global Phasing Ltd.: Cambridge, UK, 2015.
- (57) Adams, P. D.; Afonine, P. V.; Bunkóczi, G.; Chen, V. B.; Davis, I. W.; Echols, N.; Headd, J. J.; Hung, L.-W.; Kapral, G. J.; Grosse-Kunstleve, R. W.; McCoy, A. J.; Moriarty, N. W.; Oeffner, R.; Read, R. J.; Richardson, D. C.; Richardson, J. S.; Terwilliger, T. C.; Zwart, P. H. PHENIX: a Comprehensive Python-based System for Macromolecular Structure Solution. *Acta Crystallogr., Sect. D: Biol. Crystallogr.* **2010**, *66*, 213–221.
- (58) Murshudov, G. N.; Vagin, A. A.; Dodson, E. J. Refinement of Macromolecular Structures by the Maximum-Likelihood Method. *Acta Crystallogr., Sect. D: Biol. Crystallogr.* **1997**, *53*, 240–255.
- (59) Smart, O. S.; Womack, T. O.; Sharff, A.; Flensburg, C.; Keller, P.; Paciorek, W.; Vonnrhein, C.; Bricogne, G. *Grade*, version 1.2.9; Global Phasing Ltd.: Cambridge, UK, 2014.
- (60) Bruno, I. J.; Cole, J. C.; Lommerse, R. S.; Rowland, R.; Taylor, R.; Verdonk, M. L. Isostar: A Library of Information About Non-bonded Interactions. *J. Comput.-Aided Mol. Des.* **1997**, *11*, 525–537.
- (61) Chen, V. B.; Arendall, W. B., III; Headd, J. J.; Keedy, D. A.; Immormino, R. M.; Kapral, G. J.; Murray, L. W.; Richardson, J. S.; Richardson, D. C. MolProbity: All-atom Structure Validation for Macromolecular Crystallography. *Acta Crystallogr., Sect. D: Biol. Crystallogr.* **2010**, *66*, 12–21.
- (62) Davis, I. W.; Leaver-Fay, A.; Chen, V. B.; Block, J. N.; Kapral, G. J.; Wang, X.; Murray, L. W.; Arendall, W. B., 3rd; Snoeyink, J.; Richardson, J. S.; Richardson, D. C. MolProbity: All-atom Contacts and Structure Validation for Proteins and Nucleic Acids. *Nucleic Acids Res.* **2007**, *35*, W375–W383.
- (63) Obach, R. S. Potent Inhibition of Human Liver Aldehyde Oxidase by Raloxifene. *Drug Metab. Dispos.* **2004**, *32*, 89–97.